

**UCSF**

**UC San Francisco Electronic Theses and Dissertations**

**Title**

Retromer endosome exit domains serve multiple trafficking destinations and regulate local G protein activation by GPCRs

**Permalink**

<https://escholarship.org/uc/item/5pn2z1r2>

**Author**

Varandas, Katherine Varandas

**Publication Date**

2016

Peer reviewed|Thesis/dissertation



Retromer endosome exit domains serve multiple trafficking  
destinations and regulate local G protein activation by GPCRs

by

Katherine Celina Varandas

DISSERTATION

Submitted in partial satisfaction of the requirements for the degree of

DOCTOR OF PHILOSOPHY

in

Cell Biology

in the

GRADUATE DIVISION

of the

UNIVERSITY OF CALIFORNIA, SAN FRANCISCO



## **Dedication and Acknowledgements**

This work would not be possible without the help and support from a number of colleagues, friends, and family members.

First, this thesis would not have been possible without the direction and support of my thesis advisor, Dr. Mark von Zastrow. The research in the von Zastrow lab was immediately interesting to me, as it was a combination of what I had studied as an undergraduate; signaling of adrenergic receptors and endocytic membrane trafficking. But what really interested me about joining the lab was Mark's enthusiastic personality and the welcoming lab environment that he had created. Mark gave me free range in deciding on a project to pursue, which was challenging, but really allowed me to hone my scientific judgment. Once I got into the trenches of performing experiments, Mark was always engaged in helping me troubleshoot from the most minute details of experiments to the big picture of what direction to take next. Outside of the lab, Mark is a fun and relatable guy. Our experiences together in Woods Hole, on lab outings, and just chatting about in our weekly meetings were always fun. Overall, I would summarize my experience in the lab by a nightmare that I had during my third year. In the dream, Mark got into an accident and could no longer serve as my advisor. My decision was to leave graduate school. That dream illustrated that Mark is an irreplaceable figure in my graduate school experience.

Second, I would like to thank all of my lab mates, both past and present.

The von Zastrow lab was an amazing place to work because of the friends I made there. Before I even stepped foot in the lab, Alison Leaf was a mentor and friend to me. Alison was constantly providing me with advice, both solicited and unsolicited. Her zany sense of humor made her an excellent friend to share the ups and downs of graduate school with. And then came two new graduate students, Kelsie Eichel and Grace Peng. Kelsie's work ethic and scientific intuition were inspirational in the lab and her sarcasm and sincerity made her a great friend outside of the lab. Grace Peng took on the role of younger sister in the lab, distracting and taunting us in the friendliest way possible. Together, these ladies made the von Zastrow lab a really fun and productive place to work.

Additionally, many lab members provided advice, guidance, and encouragement during my time here. Stacy Henry was my rotation advisor and was the one who really showed me the ropes in the lab. Her strong work ethic and positivity were truly inspirational. Roshanak Irannejad was also quick to offer advice or teach me new techniques. Her sweet personality had a positive impact on the lab environment. Our lab manager, Aaron Marley, was also constantly acting as a cheerleader for me, encouraging me to push outside of my comfort zone and have high ambitions.

There were many other members that made the lab the fun and innovative place that it is. My experiences in the lab wouldn't be the same without the skepticism of Paul Temkin, the wisdom of Minjong Park, the kindness of Michelle Zedlitz, originality of Nina Tsvetanova, precision of Braden Lobinger, the fearlessness of Damien Julié, the hospitality of Yasunori Uchida, the strong will of Miriam Stoeber, the camaraderie of

André Lazar, and the enthusiasm of Ben Barsi-Rhyne. And of course I must thank Thanh Lam, our administrative assistant, for patiently dealing with all of my questions and needs over the years.

Third, I need to thank all of the people who made UCSF the amazing environment that it was for during the completion of this work. My thesis committee was composed of Dr. Pat O'Farrell and Dr. Robert Edwards. Pat was the first professor I worked with at UCSF during a summer rotation. Pat acted as a second advisor to me; he helped me with projects and classwork, gave me guidance on submitting my manuscript, and helped me apply for postdoctoral positions. Robert was also a beneficial member of my committee, giving me practical advice and guidance. My classmates at UCSF were also a large source of scientific inspiration and camaraderie during graduate school. My experience wouldn't have been the same without them: Elizabeth Costa, Daniel Elnatan, Shon Green, Stefan Isaac, Adam Larson, Trevor Parry, Darien Reed, Courtney Schroeder, Isaac Strong, and Elena Zehr.

Fourth, I need to thank the friends who made San Francisco a home for me over the past six years. My classmate and roommate of three years, Melissa Hendershott, was my first real friend in San Francisco. Melissa and I did everything together for the first few years of graduate school and I'm happy that I can still call Melissa one of my best friends. Through Melissa, I met two other amazing women that together formed our "urban tribe": Lauren Fish and Elizabeth Doggett. The four of us navigated and supported each other through career changes, school applications, new relationships, new homes, break-ups, make-ups, engagements, and even new marriages. Lauren and

I also mentored an amazing high school student together through Minds Matter of San Francisco, Austin Van. Getting to know Lauren and mentor Austin was an amazing experience that pushed me to pursue a career in teaching. Additionally, my classmate Andrew Lyon and I have become close friends, bonding over our love of concerts, food, and cheap or not so cheap beer.

Fifth, I need to thank my family. My father, Paul Varandas, has always pushed me to pursue education. He worked tirelessly to provide for our family with the opportunities that he didn't have as an immigrant in this country. My mother, Irene Varandas, was always there to listen when times got tough in graduate school and remains a big source of support of mine. My sister, Kimberly Varandas, and I have become very close as adults. Watching her grow and become a mother to my amazing niece, Madison Dorval, over these years has been a wonderful experience. My grandmother, Maria Celicina Varandas, was always there for me when things got tough and really acted as a second mother to me. She always welcomed me into her home, cooked me delicious meals, and gave me the most comforting hugs. My aunt Maria Jose Varandas, uncle Rui Varandas and his partner Susanne Davis, my cousins Lisa Lavin, Jacqueline Goncalves, and Briana Goncalves make every holiday and visit home special.

My greatest accomplishment outside of the lab during these years was developing a wonderful relationship with my fiancé Sam Denton-Schneider. Sam and I met in during my third year, and although we don't have much in common on paper, we developed an amazing partnership. I wouldn't be where I am today without his love, generosity, patience, and support over these past years. Sam's family has also become a family

away from home for me. Sam's parents, Jane and Jeff, and his brothers, Ben and Jonny, have generously and lovingly welcomed me into their home and their family. Additionally, Sam's uncle, John Denton, and aunt, Laura Jacobson, have been terrific roommates over the past several months and have really helped me assimilate into being a member of the Denton family.

Finally, I would like to dedicate this thesis to my grandfather, José Alberto Varandas who passed away in January of this year. Since I was a child, he always told me that I should be recognized by my surname in school as an exceptional student. He challenged me to riddles, quizzes on roman numerals, and games of cards and checkers to make sure that my wit was sharp. He was incredibly proud that there would one day be a Dr. Varandas in the family but unfortunately did not live to see it become reality.

## **Abstract**

Retromer endosome exit domains serve multiple trafficking destinations and regulate local G protein activation by GPCRs

by

Katherine Celina Varandas

This thesis asks (1) whether the divergent trafficking functions of the endosome-associating coat complex retromer require cargos to exit endosomes separately and (2) if distinct cargo-retromer interaction mechanisms affect signal activation from endosomes. My studies utilize two retromer cargos that illustrate trafficking to distinct destinations. First, the  $\beta$ -2 adrenergic receptor (B2AR) is a classical, signaling G protein-coupled receptor that responds to catecholamines and utilizes retromer for its transport from endosomes to the plasma membrane, the recycling pathway. Second, Wntless is a transport receptor for Wnt ligands, which are essential in developmental patterning and are mis-regulated in cancer, and requires retromer for its transport from endosomes to the trans-Golgi network (TGN), the retrograde transport pathway. Although my studies focus on these two cargos, the assumption is that the mechanistic insight gained is applicable to retromer-dependent transport generally. Chapter one provides an introduction to signaling and G protein-coupled receptors, explains the connection between signaling and membrane trafficking, introduces retromer, describes the model system used, and discusses previous knowledge of GPCR signaling from endosomes. Chapter two describes my findings showing that retromer mediates shared exit of cargos with divergent destinations and exerts a form of kinetic sorting that (1)



determines the rate of cargo delivery and (2) controls signal activation by B2AR at endosomes. Finally, chapter three discusses the broader meaning of these new findings, places them into the context of current knowledge, and proposes future directions of this work.

## **Table of Contents**

<b>Chapter 1: Introduction</b>	<b>1</b>
1.1 Overview	2
1.2 Cell signaling and G protein-coupled receptors	3
1.3 Membrane traffic and the regulation of cell signaling	6
1.4 Retromer and its diverse functions in mammalian cells	10
1.5 Experimental model	13
1.6 Endosomal signaling of GPCRs and the role of Retromer	15
1.7 References	17
 <b>Chapter 2: Retromer endosome exit domains serve multiple trafficking destinations and regulate signal activation by GPCRs</b>	 <b>26</b>
2.1 Summary	27
2.2 Introduction	28
2.3 Results	31
2.4 Discussion	44
2.5 Acknowledgements	48
2.6 Experimental procedures	49
2.7 References	58
2.8 Figures	65
 <b>Chapter 3: Discussion</b>	 <b>90</b>

3.1 Cargos with divergent itineraries exit endosomes together	91
3.2 Cargo-retromer interaction motifs are interchangeable in achieving each cargo's downstream destination	94
3.3 Distinct RED enrichments determine cargo delivery kinetics and signal activation at endosomes	97
3.4 Proposed mechanisms for sorting downstream of endosome exit	100
3.5 A distinct Wls cytoplasmic tail	104
3.6 References	108
3.7 Figures	113

## List of Figures

### Chapter 2

- Figure 1.** Direct comparison of retromer-dependent recycling and retrograde transport cargos in the same cells. 77
- Figure 2.**  $\beta$ 2AR and WIs traffic through the same endosomes and retromer endosome domains. 78
- Figure 3.**  $\beta$ 2AR and WIs have distinct abilities to enrich in and exit from REDs. 79
- Figure 4.** Identification of  $\Phi$ -X-[L/M] motifs in WIs' cytoplasmic tail required for strong RED enrichment and retrograde transport. 80
- Figure 5.** WIs' and  $\beta$ 2AR's cytoplasmic tails determine RED enrichment and trafficking kinetics, but not target destination. 81
- Figure 6.**  $\beta$ 2AR and WIs are each able to transit both the plasma membrane and the TGN. 82
- Figure 7.**  $\beta$ 2AR mutant RED enrichment is inversely correlated with G protein activation at endosomes. 83
- Figure S1.** Topology and localization of additional epitope-tagged WIs constructs. 84
- Figure S2.** Relative expression levels of epitope tagged  $\beta$ 2AR and WIs and assessment of co-expression on membrane trafficking. 85
- Figure S3.** Structured illumination microscopy (SIM) confirms  $\beta$ 2AR and WIs have distinct abilities to enrich in REDs. 86
- Figure S4.** Bipartite nature of the retromer sorting determinant in the WIs cytoplasmic tail. 87

**Figure S5.** Cytoplasmic tail swapping between  $\beta$ 2AR and Wls does not change downstream destination. 88

**Figure S6.** B2AR mutant constructs are functional in signaling assays and do not significantly alter the fraction cAMP produced from endosomes. 89

### **Chapter 3**

**Figure 1.** Wls2 traffics differently than Wls. 114

**Figure 2.** Examination of Wls2's PDZ motif and its localization on multivesicular bodies. 115

## **Chapter 1: Introduction**

## 1.1 Overview

This dissertation focuses on elucidating whether the distinct trafficking functions of the endosome-associating membrane coat complex retromer require cargos to be recognized and packaged into distinct sorting intermediates. We specifically focused on cargos relevant to cellular signaling, the beta-2 adrenergic receptor, a prototypical G protein-coupled receptor, and Wntless, the Wnt ligand transport protein. Additionally, we asked whether retromer's interaction with G protein-coupled receptors affects their cell signal activation from endosomes. The introduction provides an overview of cellular signaling and G protein-coupled receptors, describes how cellular signaling is regulated by membrane trafficking events, summarizes previous knowledge of retromer, describes the experimental model used, and discusses previous knowledge of G protein-coupled receptor trafficking at endosomes.

## **1.2 Cell signaling and G protein-coupled receptors**

Cells are the smallest unit of life and can exist on their own or function in groups to compose multicellular organisms. Cells sense their environment and communicate with one another via cellular signaling.

The external signals that the cell can receive, collectively termed ligands, are extremely diverse and include ions, small molecules, peptides, and proteins. Cells must transduce the presence of these external ligands to the inside of the cell, and therefore across the cell membrane, and utilize receptor proteins to do so. Receptors pass through the cell membrane bind and to the extracellular ligands. Receptor-ligand binding induces a changes to the intracellular portion of the receptor, indicating the presence of the external ligand and initiating the signaling event (Alberts et al. 2014).

There are many types of receptor proteins, which can be grouped into three main classes: (1) ion channel-coupled receptors, (2) enzyme-coupled receptors, and (3) G protein-coupled receptors (GPCRs). This thesis focuses on GPCRs, which are the largest family of cell-surface receptors, encoding for over 800 proteins in humans or 2% of the human genome. GPCRs mediate signaling in response to a vast array of ligands such as photons of light, odorants, hormones, growth factors, and neurotransmitters to support diverse responses including vision, smell, behavioral regulation, growth and



patterning, and thought and mood, respectively. Additionally, almost half of pharmaceutical drugs and many illicit drugs target GPCRs (Alberts et al. 2014).

Despite their incredible functional diversity, GPCRs have a unified structure and mechanism of activation. GPCRs pass through the cell membrane seven times, forming a cylindrical structure that often allows for ligand binding at its center. Upon ligand binding, the orientation of the seven transmembrane domains changes, allowing the internal surfaces of the receptor to activate intracellular heterotrimeric G proteins. The three subunits that compose these heterotrimeric G proteins are  $\alpha$ ,  $\beta$ , and  $\gamma$ . The  $G\alpha$  subunit is a GTPase, which is inactive when bound to GDP and active when bound to GTP. The “switch-like” activation of the  $G\alpha$  protein is stimulated by a guanine nucleotide exchange factor, in this case the GPCR itself, which displaces the GDP molecule and allows GTP to bind in its place.  $G\alpha$  undergoes conformational change upon GTP binding that releases the G protein from the GPCR and also causes dissociation of  $G\beta\gamma$ . The activated  $G\alpha$  and  $G\beta\gamma$  are then free act on downstream targets such as enzymes and ion channels (Alberts et al. 2014).

Several types of  $G\alpha$  proteins regulate the production of critical second messenger, cyclic AMP (cAMP). Stimulatory G proteins ( $G_{\alpha s}$ ) stimulate the production of cAMP while inhibitory G proteins inhibit the production of cAMP, by either activating or inhibiting the cAMP-producing enzymes, adenylyl cyclases. The concentration of cellular cAMP is constantly being regulated the opposing actions of adenylyl cyclases,

which produce cAMP, and phosphodiesterases, which break down cAMP. The activation of a G $\alpha$ s-coupled GPCR can cause an intracellular cAMP increase of more than twenty-fold in seconds. cAMP accumulation activates cAMP-dependent protein kinase A, which has downstream targets that widely vary depending on cell type, initiating a vast array of cAMP mediated responses including the secretion of hormones, the metabolism of macromolecules, or the regulation of heart function. Some of these responses occur quickly, such as the rapid cascade of enzymatic reactions which can occur within seconds, while other require transcriptional responses which can take several hours to fully develop (Alberts et al. 2014).

### **1.3 Membrane traffic and its regulation of cell signaling**

In order for cells to function properly, their components must be precisely localized. This is particularly evident in the case of signaling molecules, including membrane embedded receptors and their cognate ligands, which must be correctly localized to contact one another and initiate signal activation.

Eukaryotic cells have evolved an extensive network of endomembrane bound compartments that spatially and temporally segregate their biological processes. The movement of molecules between these compartments precisely controls their identity, composition, and activity. Membrane-embedded and many luminal proteins, including signaling receptors and secreted ligands, are synthesized at the endoplasmic reticulum (ER), modified and sorted at the Golgi apparatus, and then traffic to the plasma membrane or other intracellular location. Membrane traffic out of the ER and Golgi is collectively called the biosynthetic trafficking pathway (Alberts et al. 2014). In opposition to the biosynthetic trafficking pathway is the endocytic trafficking pathway, which moves molecules from the plasma membrane or extracellular space into the cell. The endocytic trafficking pathway begins with endocytosis, the process by which the plasma membrane forms vesicles filled with extracellular material for uptake into the cell. Endocytosis allows the cell to take up materials it needs from the extracellular environment and change the composition of the plasma membrane, including the number and type of signaling receptors present (Alberts et al. 2014).

For GPCRs, endocytic trafficking represents an important point of regulation that is shared by many GPCRs. The cascade leading to GPCR endocytosis begins with activation of the receptor which leads to phosphorylation of the receptor's intracellular domains by G protein-coupled receptor kinases. Once phosphorylated, the receptors can then interact with arrestin proteins, which halt G protein-mediated signaling by preventing further interaction with G proteins (Premont & Gainetdinov 2007). Arrestins serve as adaptor proteins for GPCRs to promote their clustering into clathrin-coated pits, the coated structures on the plasma membrane that cluster cargos for endocytosis (Hanyaloglu & von Zastrow 2008). Receptor endocytosis has long been viewed as a way to terminate signaling, as it moves the receptor off of the plasma membrane where it encounters extracellular ligands. However, this view has been challenged, first for epidermal growth factor receptors (Miaczynska et al. 2004), and more recently for GPCRs (Irannejad et al. 2013; Tsvetanova & von Zastrow 2014; Tsvetanova et al. 2015), which is discussed further in Chapter 1.6.

There are several routes that cargos, including receptors, can be “sorted” into once they are at endosomes: (1) recycling back to the plasma membrane, (2) targeting to lysosomes for degradation, and (3) retrograde transport to the trans-Golgi network (TGN). Receptors that undergo recycling can then contact subsequent rounds of ligand, allowing the cell to respond again or “resensitizing” the cell. Conversely, receptors that undergo degradation at lysosomes reduce the cell's ability to respond to that ligand

again or “desensitize” the cell (Hanyaloglu & von Zastrow 2008). Therefore, the targeting of receptors to these pathways is critical, as they have opposing effects on cellular signaling.

Classic literature on how membrane proteins “sort” between these pathways suggests that recycling occurs by “default”, while targeting to lysosomes is “active”. According to this view, the endosome membrane is constantly forming narrow tubule structures that have a high surface area to volume ratio and subsequently produce small vesicles that fuse to the plasma membrane (Maxfield & McGraw 2004). This allows membrane cargos to be efficiently separated from luminal cargos over many iterations; luminal cargos remain in endosomes which mature into lysosomes while membrane cargos recycle to the plasma membrane (Mayor et al. 1993; Dunn et al. 1989). Membrane protein cargos targeted to lysosomes require uptake into endosomes on small vesicles by the ESCRT machinery, allowing them to be treated as luminal cargos (Hanyaloglu & von Zastrow 2008). The view that recycling occurs by default is further supported by studies showing that disrupting trafficking of cargos to lysosomes, or the yeast equivalent, vacuoles, causes enhanced recycling (Davis et al. 1993; Bilodeau et al. 2002; Babst et al. 2000).

However, it was later found that the beta-2 adrenergic receptor (B2AR), a prototypical GPCR, requires a specific amino acid sequence in its cytoplasmic tail for endosome-to-plasma membrane recycling, indicating the existence of a

sequence-directed form of recycling (Cao et al. 1999; Cong et al. 2001; Gage et al. 2001). The B2AR is physically separated from bulk recycling cargos at the endosome, into a distinct subset of endosomal tubules that are marked by actin, and this localization requires the amino acid recycling sequence (Puthenveedu et al. 2010). The amino acid sequence within B2AR conforms to a PDZ binding motif and interacts with the PDZ domain within sorting nexin 27 (SNX27), which is also required for efficient B2AR recycling (Lauffer et al. 2010). Interestingly, these tubule structures are marked by the endosomal coat complex retromer, and both B2AR's PDZ binding motif and SNX27 are required for entry into these retromer-marked tubules (Temkin et al. 2011). Additionally, retromer is required for the efficient recycling of B2AR (Temkin et al. 2011).

## 1.4 Retromer and its diverse functions in mammalian cells

It was very surprising when Retromer was implicated in the recycling of cargos from endosomes to the plasma membrane, as retromer had previously been shown to mediate endosome to Golgi retrograde transport. The landmark paper that first described retromer in yeast showed that retromer: (1) is a heteropentameric complex composed of a VPS26/ 29/ 35 trimer and a VPS5/ 17 dimer, (2) is present on regions of the endosome that appear to be budding, (3) is required for the correct localization of Vps10p, a yeast vacuolar hydrolase sorting receptor (Seaman et al. 1998). It was later shown that retromer sorts proteins away from the maturing endosome to the Golgi and that cargo-retromer interactions are required for this sorting (Nothwehr et al. 2000).

Retromer is deeply conserved and was shown to also mediate retrograde transport in mammalian cells (Bonifacino & Hurley 2008). There are, however, several important differences between yeast and mammalian retromer. First, the number of retromer proteins in mammals is expanded. The homologues of yeast VPS5 and VPS17, which later were classified as sorting nexin (SNX) -BAR proteins that form banana-shaped dimers that deform the membrane, are expanded in mammals and include SNX1, SNX2, SNX5, and SNX6 (Horazdovsky et al. 1997; Griffin et al. 2005; Rojas et al. 2007; Wassmer et al. 2007; Carlton et al. 2004). The homologues of yeast VPS26/ 29/ 35 trimer, later termed the cargo recognition complex for its role in recognizing sequences within cargo proteins, is also expanded as VPS26 has two human paralogs (Gallon et

al. 2015; Kerr et al. 2005). Second, the interaction between the SNX-BAR dimer and VPS26/ 29/ 35 trimer are less robust and, therefore, the mammalian VPS26/ 29/ 35 trimer will hereafter be referred to as simply retromer (Gallon et al. 2015). Third, mammalian retromer does not directly interact with many of its cargo proteins, but instead requires the adaptor or accessory proteins (Gallon et al. 2015). Fourth, mammalian retromer has a number of functions additional to its role in mediating retrograde transport, most notably in endosome to plasma membrane recycling. It is important to also note that there is evidence that retromer-dependent recycling occurs directly from the plasma membrane and does not require that cargos are first transported to the TGN (Yudowski et al. 2009; Choy et al. 2014). Fifth, mammalian retromer associates with many adaptor and accessory proteins, such as SNX27, and has been proposed to form distinct complexes with these proteins (Gallon et al. 2015).

Many retromer accessory proteins are members of the SNX protein family, which are defined by the presence of Phox homology domains (Teasdale & Collins 2012). Phox homology domains bind to specific phosphoinositides, most commonly to phosphatidylinositol 3-phosphate (PI3P) which is found at the endosome membrane. Sorting nexin 27, discussed previously in chapter 1.3, is a member of the SNX family. Since B2AR was found to utilize SNX27 as a retromer adaptor protein, several hundreds of other potential SNX27 cargo proteins have been identified (Steinberg et al. 2013). Another SNX retromer accessory protein is SNX3, which is required for retromer-dependent retrograde transport of the Wnt ligand transport receptor, Wntless



(Wls) (Yang et al. 2008; Pan et al. 2008; Belenkaya et al. 2008; Port et al. 2008; Franch-Marro et al. 2008), (Harterink et al. 2011; Zhang et al. 2011). Wls binds to Wnt proteins in the ER and chaperones them to the plasma membrane for secretion (Yu et al. 2014; Bänziger et al. 2006; Goodman et al. 2006; Bartscherer et al. 2006).

Together, these data have led a widely proposed model in which retromer instructs cargos to distinct destinations by generating pathway-dedicated retromer exit structures, referred to here as retromer endosome domains (REDs), and selecting appropriate cargos by distinct cargo-retromer interaction sequences. (Harterink et al. 2011; Johannes & Wunder 2011; van Weering et al. 2010). This model predicts that (1) retromer is able to physically separate cargos prior to endosome exit and (2) retromer biochemically distinguishes and cargos with distinct destinations for sorting into these distinct structures. This thesis directly tests the predictions of this model.

## 1.5 Experimental model

In order to test the predictions of this model, we selected two retromer cargos that have distinct, retromer-dependent recycling and retrograde transport itineraries that are important for the physiology of each: B2AR and Wls, respectively.

B2AR has long been used as a model GPCR and was the first, and therefore the most extensively characterized, retromer-dependent recycling cargo described. B2AR recycling is required for its sustained signaling in response to catecholamines such as adrenaline (Pippig et al. 1995; Lefkowitz et al. 1998). Signaling of the B2AR is required for many physiological responses including regulation of smooth muscle contraction and the control of cardiac function (Brodde et al. 2006). As such, diseases which arise from misregulation of these processes, such as asthma and heart diseases, are treated by drugs that affect B2AR signaling (Bond et al. 2007).

Wnt signaling regulates fundamental developmental processes in animals including tissues patterning, cell migration, and cell proliferation and its misregulation can lead to diseases including cancer (Port & Basler 2010). Wnt proteins are lipid-modified, secreted ligands (Port & Basler 2010). Wls was first described as a protein required for Wnt secretion and was found to have eight transmembrane domains. (Bänziger et al. 2006; Bartscherer et al. 2006; Goodman et al. 2006). Before Wls was identified, genetic screens showed that retromer is required in Wnt signaling (Coudreuse et al. 2006;

Prasad & Clark 2006). Later, the connection was made that retromer is required to transport Wntless from endosomes to the TGN in order for efficient Wnt secretion to occur (Franch-Marro et al. 2008; Port et al. 2008; Belenkaya et al. 2008; Pan et al. 2008; Yang et al. 2008). Then, Wls was found to contain a conserved endocytosis motif that is also required for its endocytosis and, when mutated, has Wnt loss of function phenotypes (Gasnereau et al. 2011). Finally, it was found that subsequent to endosome to TGN retrograde transport, Wls is transported back to the ER by a C-terminal retrieval motif, and that this step is also required for efficient Wnt secretion (Yu et al. 2014). Together, these data led to a model in which Wls: (1) binds to hydrophobic, lipid-modified Wnt ligands in the ER and traffics bound to ligands through the biosynthetic pathway to the plasma membrane where the ligands are released, (2) undergoes clathrin-mediated endocytosis, (3) undergoes retromer-dependent retrograde transport to the TGN, and (4) is retrieved to the ER for binding to subsequent Wnt ligands.

In addition to being physiologically important and taking divergent, retromer-dependent trafficking pathways, we chose Wls and B2AR as model cargos for several reasons. The first is that they have similar membrane topology; both proteins have at least seven transmembrane domains, which could facilitate swapping of trafficking motifs between the cargos. Second, these cargos illustrate the importance of membrane trafficking in cellular signaling because the localization of both receptors and ligands is affected.

## 1.6 Endosomal signaling of GPCRs and the role of Retromer

Classically, the endocytosis of GPCRs was believed to terminate G protein-mediated signaling for several reasons (Miaczynska et al. 2004; Tsvetanova et al. 2015). First, receptors are assumed to be highly phosphorylated, and therefore unable to activate G proteins, at endosomes. Second, mutations that prevent interaction of B2AR with GRKs and arrestins reduce its endocytosis but increase cAMP accumulation. Third, the acidic environment of the endosome is believed to prevent the interaction of GPCRs with their ligands (Tsvetanova & von Zastrow 2014).

However, studies in mammalian cells began to suggest that there may be G protein mediated signaling by GPCRs at endosomes. Early studies showed a second wave of GPCR signaling that was insensitive to removal of ligand from the extracellular space (Tsvetanova & von Zastrow 2014; Mullershausen et al. 2009; Calebiro et al. 2009; Ferrandon et al. 2009). Then, a non-canonical mechanism of sustained signaling through complexes containing G $\beta\gamma$  subunits and arrestin was demonstrated (Wehbi et al. 2013; Feinstein et al. 2013).

Evidence for canonical GPCR signaling through G proteins was first demonstrated for the D<sub>1</sub> dopamine receptor; endocytic inhibitors were shown to reduce cAMP production (Kotowski et al. 2011). Later, single chain antibodies that detected specific protein conformations (nanobodies) facilitated the direct detection of both active conformations

of both B2AR and Gαs at endosomes (Irannejad et al. 2013). cAMP produced from endosomal B2ARs was later shown to have transcriptional consequences (Tsvetanova & von Zastrow 2014).

Interestingly, it was suggested that retromer was able to terminate cAMP signals produced from distinct GPCRs at endosomes (Feinstein et al. 2011; Feinstein et al. 2013) . Additionally, enhanced endosomal dwell time of several GPCRs was shown to increase signaling from endosomes (Chan et al. 2016; Tian et al. 2016). Therefore, I was interested in how retromer regulated endosomal signaling of GPCRs.

## 1.7 References

Alberts, B. et al., 2014. *Molecular Biology of the Cell, Sixth Edition*, Garland Science.

Babst, M. et al., 2000. Mammalian tumor susceptibility gene 101 (TSG101) and the yeast homologue, Vps23p, both function in late endosomal trafficking. *Traffic*, 1(3), pp.248–258.

Bänziger, C. et al., 2006. Wntless, a Conserved Membrane Protein Dedicated to the Secretion of Wnt Proteins from Signaling Cells. *Cell*, 125(3), pp.509–522.

Bartscherer, K. et al., 2006. Secretion of Wnt ligands requires Evi, a conserved transmembrane protein. *Cell*, 125(3), pp.523–533.

Belenkaya, T.Y. et al., 2008. The retromer complex influences Wnt secretion by recycling wntless from endosomes to the trans-Golgi network. *Developmental cell*, 14(1), pp.120–131.

Bilodeau, P.S. et al., 2002. The Vps27p Hse1p complex binds ubiquitin and mediates endosomal protein sorting. *Nature cell biology*, 4(7), pp.534–539.

Bond, R.A. et al., 2007. Getting to the heart of asthma: can “beta blockers” be useful to treat asthma? *Pharmacology & therapeutics*, 115(3), pp.360–374.

Bonifacino, J.S. & Hurley, J.H., 2008. Retromer. *Current opinion in cell biology*, 20(4), pp.427–436.

- Brodde, O.-E., Bruck, H. & Leineweber, K., 2006. Cardiac adrenoceptors: physiological and pathophysiological relevance. *Journal of pharmacological sciences*, 100(5), pp.323–337.
- Calebiro, D. et al., 2009. Persistent cAMP-signals triggered by internalized G-protein-coupled receptors. *PLoS biology*, 7(8), p.e1000172.
- Cao, T.T. et al., 1999. A kinase-regulated PDZ-domain interaction controls endocytic sorting of the beta2-adrenergic receptor. *Nature*, 401(6750), pp.286–290.
- Carlton, J. et al., 2004. Sorting nexin-1 mediates tubular endosome-to-TGN transport through coincidence sensing of high- curvature membranes and 3-phosphoinositides. *Current biology: CB*, 14(20), pp.1791–1800.
- Chan, A.S.M. et al., 2016. Sorting nexin 27 couples PTHR trafficking to retromer for signal regulation in osteoblasts during bone growth. *Molecular biology of the cell*, 27(8), pp.1367–1382.
- Choy, R.W.-Y. et al., 2014. Retromer mediates a discrete route of local membrane delivery to dendrites. *Neuron*, 82(1), pp.55–62.
- Cong, M. et al., 2001. Binding of the beta2 adrenergic receptor to N-ethylmaleimide-sensitive factor regulates receptor recycling. *The Journal of biological chemistry*, 276(48), pp.45145–45152.
- Coudreuse, D.Y.M. et al., 2006. Wnt gradient formation requires retromer function in

- Wnt-producing cells. *Science*, 312(5775), pp.921–924.
- Davis, N.G., Horecka, J.L. & Sprague, G.F., Jr, 1993. Cis- and trans-acting functions required for endocytosis of the yeast pheromone receptors. *The Journal of cell biology*, 122(1), pp.53–65.
- Dunn, K.W., McGraw, T.E. & Maxfield, F.R., 1989. Iterative fractionation of recycling receptors from lysosomally destined ligands in an early sorting endosome. *The Journal of cell biology*, 109(6 Pt 2), pp.3303–3314.
- Feinstein, T.N. et al., 2013. Noncanonical control of vasopressin receptor type 2 signaling by retromer and arrestin. *The Journal of biological chemistry*, 288(39), pp.27849–27860.
- Feinstein, T.N. et al., 2011. Retromer terminates the generation of cAMP by internalized PTH receptors. *Nature chemical biology*, 7(5), pp.278–284.
- Ferrandon, S. et al., 2009. Sustained cyclic AMP production by parathyroid hormone receptor endocytosis. *Nature chemical biology*, 5(10), pp.734–742.
- Franch-Marro, X. et al., 2008. Wingless secretion requires endosome-to-Golgi retrieval of Wntless/Evi/Sprinter by the retromer complex. *Nature cell biology*, 10(2), pp.170–177.
- Gage, R.M. et al., 2001. A transplantable sorting signal that is sufficient to mediate rapid recycling of G protein-coupled receptors. *The Journal of biological chemistry*,



276(48), pp.44712–44720.

Gallon, M., Matthew, G. & Cullen, P.J., 2015. Retromer and sorting nexins in endosomal sorting. *Biochemical Society transactions*, 43(1), pp.33–47.

Gasnereau, I. et al., 2011. Identification of an Endocytosis Motif in an Intracellular Loop of Wntless Protein, Essential for Its Recycling and the Control of Wnt Protein Signaling. *The Journal of biological chemistry*, 286(50), pp.43324–43333.

Goodman, R.M. et al., 2006. Sprinter: a novel transmembrane protein required for Wg secretion and signaling. *Development*, 133(24), pp.4901–4911.

Griffin, C.T., Trejo, J. & Magnuson, T., 2005. Genetic evidence for a mammalian retromer complex containing sorting nexins 1 and 2. *Proceedings of the National Academy of Sciences of the United States of America*, 102(42), pp.15173–15177.

Hanyaloglu, A.C. & von Zastrow, M., 2008. Regulation of GPCRs by endocytic membrane trafficking and its potential implications. *Annual review of pharmacology and toxicology*, 48, pp.537–568.

Harterink, M. et al., 2011. A SNX3-dependent retromer pathway mediates retrograde transport of the Wnt sorting receptor Wntless and is required for Wnt secretion. *Nature cell biology*, 13(8), pp.914–923.

Horazdovsky, B.F. et al., 1997. A sorting nexin-1 homologue, Vps5p, forms a complex with Vps17p and is required for recycling the vacuolar protein-sorting receptor.

- Molecular biology of the cell*, 8(8), pp.1529–1541.
- Irannejad, R. et al., 2013. Conformational biosensors reveal GPCR signalling from endosomes. *Nature*, 495(7442), pp.534–538.
- Johannes, L. & Wunder, C., 2011. The SNXy flavours of endosomal sorting. *Nature cell biology*, 13(8), pp.884–886.
- Kerr, M.C. et al., 2005. A Novel Mammalian Retromer Component, Vps26B. *Traffic*, 6(11), pp.991–1001.
- Kotowski, S.J. et al., 2011. Endocytosis Promotes Rapid Dopaminergic Signaling. *Neuron*, 71(2), pp.278–290.
- Lauffer, B.E.L. et al., 2010. SNX27 mediates PDZ-directed sorting from endosomes to the plasma membrane. *The Journal of cell biology*, 190(4), pp.565–574.
- Lefkowitz, R.J. et al., 1998. Mechanisms of beta-adrenergic receptor desensitization and resensitization. *Advances in pharmacology*, 42, pp.416–420.
- Maxfield, F.R. & McGraw, T.E., 2004. Endocytic recycling. *Nature reviews. Molecular cell biology*, 5(2), pp.121–132.
- Mayor, S., Presley, J.F. & Maxfield, F.R., 1993. Sorting of membrane components from endosomes and subsequent recycling to the cell surface occurs by a bulk flow process. *The Journal of cell biology*, 121(6), pp.1257–1269.

- Miaczynska, M. et al., 2004. Not just a sink: endosomes in control of signal transduction. *Current opinion in cell biology*, 16(4), pp.400–406.
- Mullershausen, F. et al., 2009. Persistent signaling induced by FTY720-phosphate is mediated by internalized S1P1 receptors. *Nature chemical biology*, 5(6), pp.428–434.
- Nothwehr, S.F., Ha, S.A. & Bruinsma, P., 2000. Sorting of yeast membrane proteins into an endosome-to-Golgi pathway involves direct interaction of their cytosolic domains with Vps35p. *The Journal of cell biology*, 151(2), pp.297–310.
- Pan, C.-L. et al., 2008. C. elegans AP-2 and retromer control Wnt signaling by regulating mig-14/Wntless. *Developmental cell*, 14(1), pp.132–139.
- Pippig, S., Andexinger, S. & Lohse, M.J., 1995. Sequestration and recycling of beta 2-adrenergic receptors permit receptor resensitization. *Molecular pharmacology*, 47(4), pp.666–676.
- Port, F. et al., 2008. Wingless secretion promotes and requires retromer-dependent cycling of Wntless. *Nature cell biology*, 10(2), pp.178–185.
- Port, F. & Basler, K., 2010. Wnt trafficking: new insights into Wnt maturation, secretion and spreading. *Traffic*, 11(10), pp.1265–1271.
- Prasad, B.C. & Clark, S.G., 2006. Wnt signaling establishes anteroposterior neuronal polarity and requires retromer in C. elegans. *Development*, 133(9), pp.1757–1766.

- Premont, R.T. & Gainetdinov, R.R., 2007. Physiological roles of G protein-coupled receptor kinases and arrestins. *Annual review of physiology*, 69, pp.511–534.
- Puthenveedu, M.A. et al., 2010. Sequence-dependent sorting of recycling proteins by actin-stabilized endosomal microdomains. *Cell*, 143(5), pp.761–773.
- Rojas, R. et al., 2007. Interchangeable but essential functions of SNX1 and SNX2 in the association of retromer with endosomes and the trafficking of mannose 6-phosphate receptors. *Molecular and cellular biology*, 27(3), pp.1112–1124.
- Seaman, M.N., McCaffery, J.M. & Emr, S.D., 1998. A membrane coat complex essential for endosome-to-Golgi retrograde transport in yeast. *The Journal of cell biology*, 142(3), pp.665–681.
- Steinberg, F. et al., 2013. A global analysis of SNX27-retromer assembly and cargo specificity reveals a function in glucose and metal ion transport. *Nature cell biology*, 15(5), pp.461–471.
- Teasdale, R.D. & Collins, B.M., 2012. Insights into the PX (phox-homology) domain and SNX (sorting nexin) protein families: structures, functions and roles in disease. *Biochemical Journal*, 441(1), pp.39–59.
- Temkin, P. et al., 2011. SNX27 mediates retromer tubule entry and endosome-to-plasma membrane trafficking of signalling receptors. *Nature cell biology*, 13(6), pp.715–721.

- Tian, X. et al., 2016. The  $\alpha$ -Arrestin ARRDC3 Regulates the Endosomal Residence Time and Intracellular Signaling of the  $\beta$ 2-Adrenergic Receptor. *The Journal of biological chemistry*, 291(28), pp.14510–14525.
- Tsvetanova, N.G., Irannejad, R. & von Zastrow, M., 2015. G protein-coupled receptor (GPCR) signaling via heterotrimeric G proteins from endosomes. *The Journal of biological chemistry*, 290(11), pp.6689–6696.
- Tsvetanova, N.G. & von Zastrow, M., 2014. Spatial encoding of cyclic AMP signaling specificity by GPCR endocytosis. *Nature chemical biology*, 10(12), pp.1061–1065.
- Wassmer, T. et al., 2007. A loss-of-function screen reveals SNX5 and SNX6 as potential components of the mammalian retromer. *Journal of cell science*, 120(Pt 1), pp.45–54.
- van Weering, J.R.T., Verkade, P. & Cullen, P.J., 2010. SNX-BAR proteins in phosphoinositide-mediated, tubular-based endosomal sorting. *Seminars in cell & developmental biology*, 21(4), pp.371–380.
- Wehbi, V.L. et al., 2013. Noncanonical GPCR signaling arising from a PTH receptor–arrestin–G $\beta\gamma$  complex. *Proceedings of the National Academy of Sciences*, 110(4), pp.1530–1535.
- Yang, P.-T. et al., 2008. Wnt signaling requires retromer-dependent recycling of MIG-14/Wntless in Wnt-producing cells. *Developmental cell*, 14(1), pp.140–147.

Yudowski, G.A. et al., 2009. Cargo-mediated regulation of a rapid Rab4-dependent recycling pathway. *Molecular biology of the cell*, 20(11), pp.2774–2784.

Yu, J. et al., 2014. WLS retrograde transport to the endoplasmic reticulum during Wnt secretion. *Developmental cell*, 29(3), pp.277–291.

Zhang, P. et al., 2011. SNX3 controls Wingless/Wnt secretion through regulating retromer-dependent recycling of Wntless. *Cell research*, 21(12), pp.1677–1690.

## **Chapter 2: Retromer endosome exit domains serve multiple trafficking destinations and regulate local G protein activation by GPCRs**

Katherine C. Varandas and Mark von Zastrow conceived of the project. Katherine C. Varandas conducted experiments and analysis with assistance from Roshanak Irannejad and supervision from Mark von Zastrow. Katherine C. Varandas and Mark von Zastrow wrote the manuscript.

## 2.1 Summary

Retromer mediates sequence-directed cargo exit from endosomes to support both endosome-to-Golgi (retrograde transport) and endosome-to-plasma membrane (recycling) itineraries. It is not known if these trafficking functions require cargos to exit endosomes separately via distinct transport intermediates, or if the same retromer-coated carriers can support both itineraries. We addressed this question by comparing human Wntless (Wls) and  $\beta$ -2 adrenergic receptor ( $\beta$ 2AR), which require retromer physiologically for retrograde transport and recycling, respectively. We show here, by direct visualization in living cells, that both cargos transit primarily the same endosomes and exit via shared transport vesicles generated from a retromer-coated endosome domain. While both Wls and  $\beta$ 2AR clearly localize to the same retromer-coated endosome domains, Wls is consistently enriched more strongly. This enrichment difference is determined by distinct motifs present in the cytoplasmic tail of each cargo, with Wls using tandem  $\Phi$ -X-[L/M] motifs and  $\beta$ 2AR using a PDZ motif. Exchanging these determinants reverses the enrichment phenotype of each cargo but does not change cargo itinerary, verifying the multifunctional nature of retromer and implying that additional sorting must occur downstream. Quantitative differences in the degree of cargo enrichment instead underlie a form of kinetic sorting that impacts the rate of cargo delivery via both itineraries and determines the ability of  $\beta$ 2AR to activate its cognate G protein transducer locally from endosomes. We propose that mammalian retromer forms a multifunctional membrane coat that supports shared cargo exit for divergent trafficking itineraries and regulates signaling from endosomes.



## 2.2 Introduction

Retromer was discovered in *S. cerevisiae* through its role in retrieving membrane cargos from endosomes to Golgi membranes, the retrograde transport route (Seaman et al. 1998; Seaman et al. 1997). In *S. cerevisiae*, retromer is a stable heteropentamer composed of a VPS26/29/35 heterotrimer, which mediates cargo selection by binding to sorting determinants present in cargo proteins, and a VPS5/17 heterodimer that deforms the endosome membrane for vesicle budding (Seaman et al. 1998; Nothwehr et al. 2000; Horazdovsky et al. 1997).

Retromer is deeply conserved, and mutations or alterations in expression of retromer components in humans have been associated with a variety of pathologies (Trousdale et al. 2015; Haft et al. 2000; Haft et al. 1998). In mammals and other higher eukaryotes, retromer has additional trafficking functions (Gallon & Cullen 2015). Particularly, mammalian retromer supports cargo-selective endosome-to-plasma membrane recycling, as well as delivery to the trans-Golgi network (TGN)(Chen et al. 2010; Temkin et al. 2011). This recycling route is important for the regulation of various PDZ motif-bearing membrane cargos, including a number of signaling receptors (Temkin et al. 2011). Additionally, interactions between the mammalian VPS26/29/35 heterotrimer and the heterodimer of VPS5/17 homologues, the sorting nexin-BAR proteins SNX1, 2, 5, and 6, are weaker in mammals than *S. cerevisiae* (Rojas et al. 2007; Wassmer et al. 2007; Swarbrick et al. 2011). Hence, mammalian retromer is generally defined as the VPS26/29/35 trimer, which associates with additional accessory proteins that confer

specialized properties (Temkin et al. 2011; Harterink et al. 2011; Zhang et al. 2011; Gallon et al. 2014). For example, sorting nexin 27 (SNX27) is required for retromer-dependent recycling of the  $\beta$ -2 adrenergic receptor ( $\beta$ 2AR) (Temkin et al. 2011; Lauffer et al. 2010) and sorting nexin 3 (SNX3) is required for retromer-dependent retrograde transport of the Wnt ligand transport protein, Wntless (Wls) (Harterink et al. 2011; Zhang et al. 2011).

Retromer is thought to form a coated domain of the endosome limiting membrane where cargos are selected for packaging into membrane intermediates that bud from the limiting membrane and are subsequently delivered to downstream destinations (Gallon & Cullen 2015; Seaman et al. 1998). From this perspective, a fundamental question arises: how is the expanded diversity of retromer function is achieved? One possibility is that the discrete retrograde transport and recycling functions of retromer are mediated by the formation of separate retromer-containing coat complexes and exit carriers. According to this hypothesis, functional diversity of retromer is solved by the formation of biochemically distinct coat structures, each containing a different complement of accessory proteins and specialized to package recycling or retrograde cargos into distinct transport intermediates. Alternatively, retromer may have the ability to generate a multifunctional coat structure that packages cargos destined for both itineraries into shared intermediates. According to this hypothesis, retromer provides a flexible endosome exit site for multiple cargos, and must work in coordination with additional sorting downstream.

These hypotheses are not mutually exclusive but, to our knowledge, neither has been directly tested. We did so here by comparing  $\beta$ 2AR and WIs, widely expressed mammalian retromer cargos that require recycling or retrograde transport, respectively, for their normal physiological operations (Temkin et al. 2011; Franch-Marro et al. 2008; Port et al. 2008; Belenkaya et al. 2008; Pan et al. 2008; Yang et al. 2008). We asked if these retromer-dependent cargos can transit the same endosomes and, if so, if their distinct itineraries require them to exit endosomes via different retromer-coated membranes. We show directly that both cargos transit the same endosomes and exit via a shared retromer-associated region of the endosome membrane. Independently verifying this conclusion, we show that endosome exit is mediated by discrete retromer sorting determinants in  $\beta$ 2AR and WIs, but that each determinant can support both itineraries. Together, our findings support the hypothesis that mammalian retromer has the capacity to generate truly multifunctional exit structures on endosomes. We also show that retromer mediates kinetic sorting that controls the ability of  $\beta$ 2ARs to locally activate the heterotrimeric G protein, Gs, from the endosome membrane.

## 2.3 Results

### **An experimental system for comparing cargo exit from endosomes**

We focused on  $\beta$ 2AR and Wls as retromer-dependent cargos with physiological recycling and retrograde transport itineraries, respectively (Temkin et al. 2011; Franch-Marro et al. 2008; Port et al. 2008; Belenkaya et al. 2008; Pan et al. 2008; Yang et al. 2008), that require distinct accessory proteins to exit from endosomes (Lauffer et al. 2010; Harterink et al. 2011; Zhang et al. 2011).  $\beta$ 2AR and Wls are widely expressed in mammalian tissues, and are co-expressed in various cell lines including HEK-293 and HeLa cells that are widely used models of  $\beta$ 2AR signaling and trafficking (Violin et al. 2008; Yu et al. 2014; Anon n.d.; Anon n.d.).

$\beta$ 2AR was tagged in its N-terminal extracellular domain with a Flag epitope (Flag- $\beta$ 2AR; Figure 1A), shown previously not to disrupt receptor function or trafficking (Irannejad et al. 2013; von Zastrow & Kobilka 1992). Wls was tagged in its largest extracellular loop. Wild type Wls accumulates in the ER after endocytosis and retrograde transport (Franch-Marro et al. 2008; Port et al. 2008; Belenkaya et al. 2008; Pan et al. 2008; Yang et al. 2008; Gasnereau et al. 2011), and the downstream, retromer-independent step of TGN-to-ER retrieval can be specifically blocked by epitope fusion to the intracellular C-terminus (Yu et al. 2014). We verified this (Figure S1) and included a C-terminal HA epitope to generate a model cargo for examination of upstream, retromer-dependent trafficking (HA-Wls, Figure 1A). Validating this, HA-Wls was detectable in the plasma membrane by fluorescence microscopy of non-permeabilized

cells and in permeabilized cells was most highly concentrated in TGN membranes defined by colocalization with TGN46 (Figure 1B). Both Flag- $\beta$ 2AR and HA-Wls trafficking remained retromer-dependent because RNAi-mediated depletion of VPS35 caused pronounced down-regulation of both model cargos (Figure 1C).

We identified transfection conditions to achieve similar levels of both tagged proteins in the plasma membrane, determined by fluorescence flow cytometry (Figure S2A). Because HA-Wls accumulates in the TGN at steady state, total cellular HA-Wls expression had to be adjusted ~10-fold higher than  $\beta$ 2AR (Figure S2B). This corresponds to overexpression of ~5-fold relative to endogenous Wls (Figure S2B). Flag- $\beta$ 2AR expressed under similar experimental conditions was shown previously to achieve 5-10 fold overexpression relative to endogenous  $\beta$ 2AR (Cao et al. 2005; Violin et al. 2008).

We then asked if these conditions allow Flag- $\beta$ 2AR and HA-Wls to traffic differentially in the same cells. We first compared the localization of each model cargo at steady state in fixed, permeabilized cells. As expected, Flag- $\beta$ 2AR localized to the plasma membrane in the absence of agonist, and to the plasma membrane and endosomes after application of the  $\beta$ 2AR agonist isoproterenol (Figure 1D). HA-Wls localized in the plasma membrane and endosomes, but was most highly concentrated in TGN membranes devoid of detectable Flag- $\beta$ 2AR, and this was insensitive to isoproterenol (Figure 1D).

We then labeled each cargo in the plasma membrane of living cells and examined the effect of a 60 minute 'chase' incubation in the presence of isoproterenol to allow endocytosis of both Flag- $\beta$ 2AR (requires isoproterenol) and HA-WIs (constitutive) (Gasnereau et al. 2011). Cargos localized similarly in the plasma membrane before the chase incubation, and each achieved a distinct, cargo-appropriate intracellular localization pattern after the 60 minute chase (Figure 1E). We further established that co-expression of HA-WIs did not affect recycling of Flag- $\beta$ 2AR (Figure S2C) and, conversely, that co-expression of Flag- $\beta$ 2AR did not affect delivery of internalized HA-WIs to the TGN (Figure S2D and S2E). Together, these results validate the present experimental model and indicate that Flag- $\beta$ 2AR and HA-WIs can achieve distinct, cargo-appropriate itineraries within 60 minutes after endocytosis in the same cells.

### **Flag- $\beta$ 2AR and HA-WIs transit the same endosomes and retromer endosome domains**

Having devised an experimental system that recapitulates distinct retromer-dependent itineraries, we investigated whether Flag- $\beta$ 2AR and HA-WIs transit the same or different endosomes, and whether they exit via the same or different retromer-associated carriers. In cells fixed after 15 minutes of chase incubation, Flag- $\beta$ 2AR and HA-WIs localized to the same internal membrane compartments (Figure 2A). Differences in Flag- $\beta$ 2AR and HA-WIs distribution became apparent in living cells, as chemical fixation causes endosomes to collapse, and using HEK-293 cells that typically have slightly

larger endosomes (Puthenveedu et al. 2010). Again, Flag- $\beta$ 2AR and HA-WIs localized to the same compartments and most were also marked by VPS29-mCherry, defining them as retromer-associated endosomes (Figure 2B). Verifying that these heterogeneously labeled structures indeed represent the same endosomes, both model cargos moved coordinately with retromer through the cytoplasm in live image series (data not shown).

VPS29-mCherry localized to a protrusion of the endosome membrane that we generically called a 'retromer endosome domain' (RED). In the vast majority of endosomes examined, Flag- $\beta$ 2AR and HA-WIs were detected in the same REDs (Figure 2C and 2D). This was observed throughout the 60 minute chase incubation because, when images were separated into 10 min bins according to chase time, both cargos were observed in the same REDs in the majority of endosomes examined in all bins. Together, these data indicate that both Flag- $\beta$ 2AR and HA-WIs, representing model recycling and retrograde cargos, respectively, traverse the same endosomes and associate with the same REDs throughout the chase interval during which they achieve cargo-appropriate itineraries.

### **Flag- $\beta$ 2AR and HA-WIs exit endosomes via the same REDs but differ in degree of enrichment**

Flag- $\beta$ 2AR and HA-WIs differed in their relative degree of enrichment in REDs (Figures 3A and 3B). To evaluate this across multiple images and experiments, we defined a

'RED enrichment index' as the mean fluorescence signal measured per pixel in the RED divided by that in the adjacent endosome region (Figure 3C, inset). Overall, the mean RED enrichment index determined across the 60 minute chase period was 0.59 for Flag- $\beta$ 2AR and 2.60 for HA-WIs (Figure 3C). As endosomes and REDs approach the lateral resolution limit of traditional light microscopy, we used structured illumination microscopy (SIM) to achieve higher resolution (Gustafsson et al. 2008). SIM verified that Flag- $\beta$ 2AR and HA-WIs localize in the same REDs and that HA-WIs is more highly enriched in REDs than Flag- $\beta$ 2AR (Figure S3). Although SIM provides enhanced spatial resolution, we were unable to achieve sufficient temporal resolution to observed dynamic endosome movements due to slower acquisition. Therefore, we continued to utilize spinning disc confocal microscopy for subsequent analysis.

Because most REDs contained both Flag- $\beta$ 2AR and HA-WIs, we next investigated whether REDs define sites of shared cargo exit from endosomes. Small membrane vesicles were seen to bud off from REDs that contained both Flag- $\beta$ 2AR and HA-WIs and moved away from the donor endosome in live cell time series (Figure 3D). Similar to cargo enrichment in REDs, HA-WIs was more strongly enriched than Flag- $\beta$ 2AR in these exit vesicles. This was evident by line scan analysis of individual endosomes (Figure 3E) and across multiple endosomes by fluorescence intensity ratio in the exiting vesicles relative to donor endosomes (Figure 3F). Together, these observations support the hypothesis that REDs represent a region of the endosome limiting membrane where



both recycling and retrograde transport cargos are packaged for exit from endosomes via a shared population of vesicular carriers.

**A discrete sorting determinant in the Wls cytoplasmic tail that mediates cargo enrichment in REDs and is required for downstream delivery**

We next sought to understand the structural basis for differential enrichment of Flag- $\beta$ 2AR and HA-Wls in REDs.  $\beta$ 2AR associates with retromer through a C-terminal PDZ motif (Figure S4A, sequence i) that binds to SNX27 (Cao et al. 1999; Lauffer et al. 2010; Temkin et al. 2011; Franch-Marro et al. 2008)). We reasoned that Wls must utilize a different sorting determinant to engage retromer because it does not possess a PDZ motif at its C-terminus (Figure S4A, sequence ii) and can efficiently exit endosomes with an epitope tag fused to its C-terminus, a manipulation that blocks PDZ motif-directed exit of  $\beta$ 2AR from endosomes (Cao et al. 1999; Lauffer et al. 2010; Temkin et al. 2011; Franch-Marro et al. 2008).

Truncation of the distal 35 residues from the HA-Wls cytoplasmic tail (HA-Wls $\Delta$ 35; Figure S4A, sequence iii), strongly reduced enrichment in REDs relative to the parental HA-Wls construct (Figures 4A and 4B). We isolated two regions within this 35 residue region that were each sufficient to mediate increased cargo enrichment in REDs, albeit to a reduced degree when compared to parental HA-Wls containing both regions (Figure S4A, sequences iv and v; Figures S4B-D). Both regions contain a consensus  $\Phi$ -X-[L/M] motif (Seaman 2007; Tabuchi et al. 2010), and point mutating them

(HA-Wls(LQL+YKL>AAA); Figure S4A, sequence vi) reduced cargo enrichment in REDs (Figure 4C). Wls'  $\Phi$ -X-[L/M] motifs are conserved across vertebrates except zebrafish, in which the hydrophobic residue in the first motif is replaced by threonine (Figure 4D). *Drosophila* and *C. elegans* Wls both lack  $\Phi$ -X-[L/M] motifs, but contain two sequences conforming to [S/T]-X-[L/M] placed similarly in the cytoplasmic tail (Figure 4D).

We next examined whether this determinant is also required for subsequent delivery of HA-Wls to the TGN. In contrast to HA-Wls that colocalized extensively with TGN46 after 60 minute chase (Figure 4E), internalized HA-Wls $\Delta$ 35 did not (Figure 4F). Internalized HA-Wls(LQL+YKL>AAA) was also strongly impaired in delivery to the TGN (Figure 4G). These results, quantified across multiple cells and experiments by Pearson's correlation coefficient analysis (Figure 4H), indicate that the discrete sorting determinant identified in Wls is indeed necessary for accumulation of internalized HA-Wls in the TGN.

### **Cargo-specific retromer sorting determinants affect trafficking kinetics but not overall itinerary**

To investigate how discrete sorting determinants in Wls and  $\beta$ 2AR might differ, we examined the consequences of exchanging them between model cargos. The RED enrichment of internalized  $\beta$ 2AR is the same whether tagged with a HA or Flag epitope (Figure 5A), allowing mutational effects on cargo enrichment in REDs to be compared directly to that of wild type  $\beta$ 2AR in the same endosomes. When the cytoplasmic determinant identified in Wls was exchanged for the PDZ motif-containing determinant

present in Flag-β2AR, choosing junction points to maintain similar lengths of exchanged sequence to position the exchanged determinant properly, the mutant receptor (Flag-β2AR $\Delta$ 42-Wls35) enriched more strongly in the same REDs than co-expressed HA-β2AR (Figure 5B).

Remarkably, Flag-β2AR $\Delta$ 42-Wls35 recycled to the plasma membrane with efficiency indistinguishable from that of Flag-β2AR, and this was indeed a consequence of adding Wls-derived sequence rather than removing cytoplasmic sequence from β2AR (Figure 5C). Further, Flag-β2AR $\Delta$ 42-Wls35 did not accumulate in TGN membranes more than the parental Flag-β2AR (Figures S5A and S5B). Moreover, and fully consistent with its enhanced enrichment in REDs, the Wls-derived sorting determinant significantly increased the rate at which mutant β2ARs recycle to the plasma membrane (Figure 5D).

We then examined the effect of making the converse exchange, again choosing junction points to maintain similar lengths of exchanged sequence to position the exchanged determinant properly. Replacing the cytoplasmic sequence identified in Wls with that derived from β2AR (HA-Wls $\Delta$ 35-β2AR42) strongly reduced enrichment in REDs, making it indistinguishable from that observed for co-expressed Flag-β2AR (Figures 5E and 5F). However, internalized HA-Wls $\Delta$ 35-β2AR42 still strongly accumulated in the TGN after 60 minutes of chase incubation (Figure 5G, Figure S5C), and this depended on the β2AR-derived tail sequence added rather than Wls tail sequence removed (Figure 5G). Time-dependent Pearson's correlation coefficient analysis revealed that

HA-Wls $\Delta$ 35- $\beta$ 2AR42, despite localizing at long chase time in the TGN similarly to HA-Wls, accumulates there more slowly (Figure 5H). Together these data support the hypothesis that differences in cargo enrichment in REDs, as conferred by the discrete cytoplasmic sorting determinants present in each retromer cargo, dictate the rate of endosome exit and subsequent delivery to the appropriate downstream destination, but not the destination itself.

### **Evidence for downstream sorting guiding cargo itinerary after endosome exit**

Because  $\beta$ 2AR and Wls exit endosomes primarily via same REDs we next investigated trafficking events downstream of cargo exit from endosomes. Wls is considered a retrograde cargo whose delivery to the plasma membrane is assumed to occur after exit from the TGN. However, as a direct endosome-to-plasma membrane route has been clearly demonstrated for the  $\beta$ 2AR (Puthenveedu et al. 2010; Choy et al. 2014), we considered the possibility that Wls may also exhibit some ability to directly recycle. We visualized discrete vesicular insertion events into the plasma membrane by dequenching of superecliptic pHluorin (SpH) fused to the extracellular surface of cargos by rapid TIR-FM imaging as transient bursts of SpH fluorescence produced by cargo exposure to the neutral extracellular milieu (Miesenböck et al. 1998; Sankaranarayanan et al. 2000; Yudowski et al. 2006). We verified that we could visualize plasma membrane SpH-tagged  $\beta$ 2AR and that these indeed represent recycling events by coincident arrival of fluorescent antibody used to label receptors present initially in the plasma membrane (Figure 6A) (Puthenveedu et al. 2010; Yudowski et al. 2006).

Remarkably, similar insertion events were observed by imaging SpH-tagged WIs under the same conditions, and we verified that tagged WIs delivered via these insertion events also originated from the previously internalized pool by coincident arrival of surface-applied fluorescent antibody (Figure 6B). Further, the relative fluorescence intensity of SpH-tagged WIs insertion was significantly brighter than that of SpH-tagged  $\beta$ 2AR, as determined by measuring the transient fluorescence intensity increase at the site of insertion relative to ambient plasma membrane surround ( $\Delta F/F_0$ ; Figure 6C). This is consistent with the characteristically higher enrichment of WIs relative to  $\beta$ 2AR in RED-derived exit vesicles. Moreover, when surface insertion of SpH-WIs was visualized simultaneously with surface-labeled Flag- $\beta$ 2AR, both cargos were detected in the same vesicular fusion events (Figure 6D). These results support the hypothesis that plasma membrane recycling is not restricted to  $\beta$ 2AR and suggest that the recycling route is traversed by a cargo that also undergoes retrograde transport.

Conversely, while  $\beta$ 2AR undergoes endosome-to-plasma membrane recycling that bypasses the TGN, as do other various recycling cargos (Geuze et al. 1984; Snider & Rogers 1985). FAM21, a component of the WASH complex that activates Arp2/3-mediated actin polymerization at endosomes, was shown recently to also restrict TGN accumulation of PDZ motif-containing cargos, including  $\beta$ 2AR (Lee et al. 2016). We verified that FAM21 knockdown, assessed in Figure 6E, increased localization of Flag- $\beta$ 2AR in membranes marked by TGN46 (Figure 6F), albeit to a reduced degree when compared to TGN localization of HA-WIs (Figures 6G and 6H). Consistent with

this effect of FAM21 occurring downstream of endosome exit (Lee et al. 2016), FAM21 knockdown did not detectably change the localization of either Flag- $\beta$ 2AR or HA-Wls in endosomes, nor did it detectably change their distinct degrees of enrichment in shared REDs (Figures 6I and 6J).

Moreover HA-Wls $\Delta$ 35, despite lacking either retromer sorting determinant and being unable to detectably transit from endosomes to TGN (Figure 4H), was still present in the TGN when its steady state localization was assessed (Figure 6K and 6L). The source of this TGN-localized HA-Wls $\Delta$ 35 is presumably the biosynthetic pathway, and thus likely represents a mechanism of accumulation that is independent of retromer. Together, these results indicate retromer-dependent itineraries can be separated downstream of endosome exit.

### **A discrete effect of retromer sorting determinants on G protein activation from endosomes**

Because our data indicate that cargo enrichment in REDs does not dictate downstream itinerary, we wondered if these differences might have some other effect. We were particularly intrigued by the relatively weak ability of the  $\beta$ 2AR's PDZ motif-based retromer sorting determinant to drive cargo enrichment in REDs when compared to Wls'  $\Phi$ -X-[L/M] -based determinant. Because it is now evident that  $\beta$ 2AR can initiate signaling via its cognate heterotrimeric G protein, Gs, from endosomes as well as the plasma membrane (Tsvetanova & von Zastrow 2014; Irannejad et al. 2013), we asked if

this weak degree of  $\beta$ 2AR enrichment in REDs might somehow be relevant to  $\beta$ 2AR's function of signal activation at endosomes.

To do so, we applied previously validated biosensor technology to directly examine the effects of manipulating receptor enrichment in REDs on the initial steps of  $\beta$ 2AR-Gs signal activation, focusing on Flag- $\beta$ 2AR $\Delta$ PDZ that exhibits decreased RED enrichment and Flag- $\beta$ 2AR $\Delta$ 42-Wls35 that exhibits increased RED enrichment when compared to wild type Flag- $\beta$ 2AR. We first verified that these engineered receptors mediate G protein-dependent signal activation by determining that each drives ligand-dependent stimulation of cyclic AMP accumulation (Figures S6A-6C). We then specifically probed receptor activation at endosomes using a nanobody-derived biosensor (Nb80-GFP) that specifically recognizes conformationally activated receptors in living cells (Rasmussen, Choi, et al. 2011; Irannejad et al. 2013). We verified that Nb80-GFP localizes diffusely in the cytoplasm in cells not exposed to agonist and is strongly recruited to Flag- $\beta$ 2AR-containing endosomes after application of isoproterenol (Irannejad et al. 2013). The same phenomenon was observed for both Flag- $\beta$ 2AR $\Delta$ PDZ and Flag- $\beta$ 2AR $\Delta$ 42-Wls35 (Figures 7A-7C). When the degree of biosensor recruitment was quantified across images and experiments, by determining a ratio of biosensor intensity to receptor intensity at endosomes, all of the  $\beta$ 2AR-derived constructs appeared indistinguishable in their ability to be conformationally activated in endosomes (Figure 7D).

We next probed endosomal activation of Gs, the immediate downstream signal transducer in the  $\beta$ 2AR signaling cascade that is activated by direct interaction with  $\beta$ 2AR, using a different nanobody-derived biosensor (Nb37-GFP) (Rasmussen, DeVree, et al. 2011; Irannejad et al. 2013). We verified that Nb37-GFP localizes diffusely in the cytoplasm in the absence of agonist and is recruited to endosomes containing Flag- $\beta$ 2AR following application of isoproterenol (Figure 7F). Interestingly, Nb37-GFP was recruited to endosomes more strongly by Flag- $\beta$ 2AR $\Delta$ PDZ than the parental Flag- $\beta$ 2AR (Figure 7F). Conversely Flag- $\beta$ 2AR $\Delta$ 42-Wls35 failed to mediate detectable endosomal recruitment of the Gs activation biosensor in response to isoproterenol (Figure 7G). This was specific because mutating only the  $\Phi$ -X-[L/M] motifs in this construct, and thus reducing RED enrichment (Flag- $\beta$ 2AR $\Delta$ 42-Wls35(LQL+YKL>AAA)), enhanced Nb37-GFP recruitment to endosomes (Figures S6D and S6E). We verified these results across multiple images and experiments by again determining a ratio of biosensor to receptor intensity at endosomes (Figure 7H). Together, these data indicate that sequence-directed differences in the degree of  $\beta$ 2AR enrichment in REDs, while having no detectable impact on the ability of receptors to undergo conformational activation in endosomes, strongly affects the ability of receptors to subsequently activate their immediate downstream signal transducer, Gs, from the endosome membrane.



## 2.4 Discussion

This study addresses a fundamental question regarding the expanded functions of retromer observed in higher eukaryotes. Our results demonstrate that co-expressed  $\beta$ 2AR and WIs, comprising physiologically relevant recycling and retrograde cargos, localize to the same retromer-associated endosomes and can exit via the same transport intermediates generated therefrom. We also show that distinct retromer sorting determinants present in each cargo, which engage retromer through distinct mechanisms, are functionally interchangeable in their capacity to support both itineraries. We then identify a discrete type of kinetic sorting by retromer that controls the rate, but not destination, of retromer-mediated cargo exit and which influences the ability of  $\beta$ 2AR to activate its cognate signal-transducing G protein in endosomes.

The ability of  $\beta$ 2AR and WIs to achieve cargo-appropriate trafficking itineraries after shared endosome exit via REDs implies that additional sorting must occur downstream of endosome exit. We think it is likely that multiple downstream sorting operations contribute. We propose five main elements, depicted schematically in Figure 7I. First, both cargos can rapidly transit to the plasma membrane after endocytosis and both are present in the same fusing vesicles, indicating direct endosome-to-plasma membrane recycling. We note that the DMT1-II iron transporter, possessing a  $\Phi$ -X-[L/M] motif, recycles to the plasma membrane (Tabuchi et al. 2010) and speculate that DMT1-II may be a naturally occurring example of what we presently demonstrate with engineered cargos. Second, we verify that FAM21 depletion enhances TGN accumulation of  $\beta$ 2AR,

consistent with its function in suppressing PDZ motif-containing cargo delivery to the TGN (Lee et al. 2016). Third, mutant analysis indicates that structural determinants located outside of defined retromer sorting motifs determine downstream itinerary. We note that  $\beta$ 2AR and Wls differ transmembrane domain length: 23 amino acids for  $\beta$ 2AR and for 21 amino acids for Wls. These correspond closely to the average transmembrane domain lengths of plasma membrane and Golgi resident proteins in mammalian cells (Sharpe et al. 2010), and differences in transmembrane length of this order have been demonstrated previously to shift steady state cargo localization from plasma membrane to Golgi distributions (Masibay et al. 1993). Fourth, Wls has a dibasic motif located in its cytoplasmic tail that is distinct from its  $\Phi$ -X-[L/M] motifs, and which mediates a discrete, retromer-independent process of Golgi-to-ER retrieval (Yu et al. 2014). We deliberately disabled this motif in the present study to prevent this retromer-independent step, which plays a major role in distinguishing the downstream itinerary of Wls from  $\beta$ 2AR under normal physiological conditions, to focus on the upstream endosome exit step. Fifth, Wls present in the plasma membrane undergoes rapid and constitutive endocytosis, which provides a means by which Wls delivered to the plasma membrane could be retrieved and sorted again. Accordingly, constitutive endocytosis of Wls would enable an error-checking function of the sorting network and allow the physiologically appropriate retrograde itinerary of Wls to be repeatedly refined through iteration.

The discrete sorting determinants in  $\beta$ 2AR and WIs differ markedly in the degree to which they promote cargo enrichment in REDs. Our results demonstrate this to a spatial resolution of  $\sim 100$  nm; future studies using higher-resolution methods could further solidify this point. This difference mediates a type of kinetic sorting affecting the rate of cargo delivery via both recycling and retrograde routes, but does not dictate downstream cargo itinerary.

Our results also reveal an inverse correlation between B2AR enrichment in REDs and local G protein activation from endosomes. They do not, however, establish whether RED enrichment affects overall cellular signaling. The total cAMP response mediated by all of the B2AR constructs tested was partially inhibited by acute endocytic blockade imposed by Dyngo-4a, but we were unable to detect a statistically significant difference in this metric between constructs with distinct RED enrichments (Figure S6E). Receptor enrichment in REDs is expected to both reduce G protein activation from endosomes and increase it from the plasma membrane (through recycling and resensitization), creating opposing effects that are both inhibited by Dyngo-4a. Therefore, determining whether or how differential RED enrichment impacts downstream signaling remains an important direction for future study.

In sum, the present results establish that divergent recycling and retrograde trafficking itineraries can be achieved by shared cargo exit from endosomes, using a shared and likely biochemically heterogeneous retromer coat structure, and reveal a previously

unrecognized type of kinetic sorting mediated by retromer that has both trafficking and signaling consequences (Figure 7J). In addition to providing insight to functional diversity of retromer in higher eukaryotes, these findings have implications for understanding diseases caused by mutations or altered expression of retromer subunits (Trousdale et al. 2015) that have been interpreted, mainly according to effects on retrograde membrane transport.

## **2.5 Acknowledgements**

We thank Robert Levenson for providing the Wls antibody. We thank Aaron Marley and Daniel Elnatan for cloning advice and Braden Lobingier for devising the RED enrichment index metric. We thank Pat O'Farrell, Robert Edwards, David Mavor, and members of the MvZ lab for useful discussion. We thank DeLaine Larsen for assistance with imaging experiments. TIR-FM and SIM imaging experiments were carried out at the UCSF Nikon Imaging Center directed by Kurt Thorn. The work was supported by US National Institutes of Health (DA036290 to KV, HL122508 to RI, and DA012864 and DA010711 to MvZ).

## **2.6 Experimental Procedures**

Materials (DNA constructs, siRNAs, and antibodies), SIM imaging, image analysis, immunoblotting, and cAMP assays are described in Supplemental Experimental Procedures.

### **Cell culture and transfection**

HEK-293 and HeLa cells (ATCC) were grown in DMEM (Gibco) supplemented with 10% fetal bovine serum (UCSF Cell Culture Facility). Transfection of DNA constructs and siRNAs was performed using Lipofectamine 2000 and RNAi-max (Invitrogen), respectively, according to the manufacturer's instructions. For DNA expression, cells were transfected 48 hours before experiments and for siRNA knockdown, cells were transfected 72 hours before experiments.

### **Fixed Cell Microscopy**

Cells were transfected with the indicated siRNAs and/or DNA construct(s), re-plated onto glass coverslips coated with poly-L-lysine 24 hours post-transfection, and fixed for imaging 24 hours after re-plating. For surface chase assays, cells were: (1) placed on ice and rinsed with ice-cold phosphate-buffered saline (PBS), (2) labeled by the addition of antibodies in ice-cold PBS for 30 minutes, (3) rinsed with room temperature PBS, and (4) allowed to traffic for specified time point by the addition of 37°C media with or without a saturating concentration of  $\beta$ 2AR agonist (10 $\mu$ M

isoproterenol, Sigma). Cells were then rinsed with PBS and fixed by incubation in 3.7% formaldehyde (Fisher Scientific) diluted in modified BRB80 buffer (80mM PIPES, 1mM  $MgCl_2$ , 1mM  $CaCl_2$ , pH 6.8) for 15 minutes and then blocked in blocking buffer (3% Bovine Serum Albumin (Sigma) in PBS with or without permeabilization by 0.1% triton X-100 (Sigma)) for 30 minutes. Primary labeling was performed by the addition of antibodies diluted 1:1000 in blocking buffer for one hour and secondary labeling was performed by the addition of antibodies diluted at 1:500 in blocking buffer for 20 minutes. DAPI counterstaining was performed by exposing cells to 300 nM DAPI-dihydrochloride (Sigma) for one minute. Specimens were mounted using ProLong Gold antifade reagent (Life Technologies).

### **Live cell microscopy**

Cells were transfected as indicated, re-plated onto glass bottom dishes (MatTek) coated with poly-L-lysine (Sigma) 24 hours post-transfection, and imaged 24 hours post re-plating. Surface Flag and HA epitopes were labeled on ice as described above, but with Alexa Fluor-conjugated antibodies. Cells were imaged in DMEM without phenol red (UCSF Cell Culture Facility) supplemented with 30mM HEPES at 37°C.

### **Image acquisition**

Spinning disc confocal images were acquired on a Nikon TE-2000 with confocal scanner unit (Yokogawa) using a 100X NA1.45 objective using an electron multiplying CCD camera (Andor) controlled by Micro-Manager software

(<https://www.micro-manager.org>). Epifluorescence images were acquired on a Nikon inverted microscope with a 60X NA1.4 objective illuminated by a mercury arc lamp through standard dichroic filter sets (Chroma) and collected using a cooled CCD camera (Princeton Instruments). TIR-FM images were collected on a Nikon Ti-E inverted microscope equipped for through-the-objective TIR-FM with a Apo TIRF 100X, NA1.49 objective (Nikon) with solid-state lasers of 405, 488, 561 and 647 nm (Keysight Technologies) using an EMCCD camera (Andor) controlled by NIS-Elements 4.1 software to acquire image sequences every 50 ms for 5 min. Exposure times and illumination were adjusted to remain in the dynamic range of each camera.

### **Flow Cytometry and Recycling Assays**

Cells were transfected as described, re-plated into 12-well dishes 24 hours post-transfection, and analyzed by flow cytometry 24 hours post re-plating. Surface expression was measured by the addition of antibody diluted in PBS at 4°C for 25 minutes. Flow-cytometry-based recycling assays were performed as described previously (Temkin et al. 2011). Fluorescence intensity profiles of cell populations (>2,500 cells per sample) were measured using a FACS-Calibur instrument (BD Biosciences). In each experiment, duplicate treatments were analyzed for each condition.

### **DNA constructs**



Flag- $\beta$ 2AR (Tang et al. 1999), HA- $\beta$ 2AR (von Zastrow & Kobilka 1992), VPS29-mCherry (Temkin et al. 2011), Nb80-GFP and Nb37-GFP (Irannejad et al. 2013), and Flag-SpH- $\beta$ 2AR (Yudowski et al. 2006) were described previously. HA-Wls, HA-Wls-ERretrieval, and Flag-Wls-HA were created by PCR of human Wntless cDNA (Open Biosystems) to add an internal HA or Flag epitope and restriction sites followed by ligation into pIRESneo3 with or without C-terminal HA tag. HA-Wls deletion constructs (HA-Wls $\Delta$ 35, HA-Wls $\Delta$ 518-541, and HA-Wls $\Delta$ 506-518) and Flag- $\beta$ 2AR deletion constructs (Flag- $\beta$ 2AR $\Delta$ PDZ and Flag- $\beta$ 2AR $\Delta$ 42) were created by Phusion PCR amplification and blunt-end ligation (Phusion Site-Directed Mutagenesis Kit, Thermo Scientific). Chimeric constructs (HA-Wls $\Delta$ 35- $\beta$ 2ARtail and Flag- $\beta$ 2AR $\Delta$ 42-Wls35), HA-SpH-Wls, Flag-B2AR $\Delta$ 42-Wls35(LQL/YKL>AAA), and HA-Wls(LQL/YKL>AAA) were created using homology directed ligation (In-Fusion HD Cloning kit, Clontech), and for HA-Wls(LQL/YKL>AAA) a gBlock (Integrated DNA technologies) with desired mutations was used for the insertion fragment.

## **siRNAs**

siRNAs were purchased from Qiagen for control (1027281), VPS35 (SI04287605), and FAM21 (custom sequence 5'- GAACAAAACCCAAGGCAAA -3').

## **Antibodies**

Commercial primary antibodies used were: mouse anti-Flag M1 (Sigma), rabbit anti-Flag (Sigma), mouse anti-HA (Covance), rat anti-HA (Roche applied science),

rabbit anti-Giantin (Covance), sheep anti-TGN46 (AbD Serotec), rabbit anti-WASH complex subunit FAM21-C (EMD Millipore), and mouse anti-GAPDH (EMD Millipore). Chicken anti-Wls was a generous gift from Dr. Robert Levenson. Commercial secondary antibodies used were: Alexa Fluor 555 or 488 donkey anti-mouse, Alexa Fluor 555 or 488 donkey anti-rabbit , Alexa Fluor 488 or 555 goat anti-rat, or Alexa Fluor 488 donkey anti-sheep (Life Technologies). Conjugated primary antibodies used for live cell imaging and flow cytometry, with dilutions used in parentheses, were mouse anti-Flag M1 antibody conjugated to Alexa Fluor 555 or 647 (Alexa Fluor protein labeling kits, Invitrogen; 1:1000), mouse anti-HA epitope 488 conjugate (Invitrogen; 1:100), and mouse anti-HA epitope 647 conjugate (Thermo Scientific; 1:100). LI-COR secondary antibodies used for immunoblotting were donkey anti-mouse IR800, donkey anti-rabbit IR680 , and goat anti-chicken IR800 (LI-COR biosciences).

### **SIM imaging**

SIM images were acquired using a Nikon Ti-E inverted microscope through an Apo TIRF 100X 1.49 NA objective (Nikon) and 3D EX V-R SIM grating (Nikon) illuminated by sapphire lasers of 488 and 561 nm (Coherent) with an Andor iXon DU897 EMCCD camera. NIS-Elements 4.12 software was used to control hardware and reconstruct images.

### **Image analysis**

Fluorescence intensity plots were measured using ImageJ software. For data plotted as % max fluorescence, % max fluorescence was calculated for each image as follows: % max fluorescence = (mean fluorescence - min fluorescence) / (max fluorescence - min fluorescence).  $\Delta F/F_0$  for TIR-FM insertion event time series was calculated as: (mean fluorescence -  $F_0$ ) /  $F_0$ , where  $F_0$  is defined as the average fluorescence in the ten frames prior to the insertion event.

To measure RED enrichment index, regions of interest (ROIs) were drawn as freehand lines 5 pixels wide around the endosome limiting membrane and down the RED. To correct for background fluorescence, the ROIs were moved to adjacent regions within the cell and the mean background fluorescence values were subtracted from the endosome and RED fluorescence values. RED enrichment index was calculated as the background subtracted RED fluorescence per pixel divided by endosome fluorescence per pixel. Exiting vesicle: endosome ratio was calculated in a similar manner, but with freehand ROIs around the endosome and exiting vesicle.

Pearson's correlation coefficient of cargo and TGN46 was measured using the Coloc2 plugin in Fiji software (<http://fiji.sc/Fiji>). ROIs were drawn around the cell of interest in the cargo channel and PCC was calculated only within cellular ROIs.

Nanobody enrichment on endosomes was calculated by drawing: (1) circular ROIs around 5 endosomes per cell in the Flag-receptor channel, (2) circular ROIs adjacent to each endosome to correct for local background fluorescence in the Flag-receptor channel, and (3) a freehand ROI around the cell in the nanobody channel. To normalize for expression levels between cells, the mean endosome enrichment in

each channel was calculated using the formula: mean endosome enrichment= (mean endosome fluorescence-local endosome background)/(mean cell fluorescence-local endosome background). The nanobody: Flag receptor ratio for each cell was calculated as the average ratio of mean endosome enrichment in the nanobody channel divided by that of the Flag channel for the 5 endosomes measured per cell. Values reported are the mean for *n* cells.

### **Immunoblotting**

Cells were transfected with siRNAs and/ or DNA constructs as indicated, grown to confluency, and lysed in a buffer of 0.2% Triton-X100, 150mM NaCl, 25mM KCl, 10mM Tris pH7.4, 1 mM EDTA supplemented with protease inhibitor cocktail (Roche). Lysates were cleared by centrifugation and protein concentration was determined by Coomassie protein assay (Thermo scientific.) Lysates were denatured by SDS sample buffer (Novex) + 0.2M Dithiothreitol. Equal total protein amounts were loaded and run on 4-12% Bis-Tris gels (NuPAGE, Invitrogen), transferred to nitrocellulose membranes, and probed by immunoblotting, first with primary antibodies as indicated, and then with secondary antibodies conjugated to infrared dyes (LI-COR). Blots were imaged on a LI-COR scanner and images were analyzed with Image Studio Lite software ([https://www.licor.com/bio/products/software/image\\_studio\\_lite/](https://www.licor.com/bio/products/software/image_studio_lite/)).

### **cAMP Assays**

Cellular cAMP was detected by two methods. The first method utilizes a luminescence-based biosensor (pGlo-20F Promega) in live HEK-293 cells treated with saturating concentrations of either isoproterenol (10 $\mu$ M) or Forskolin (2.5 $\mu$ M), as described in Irannejad, et al., 2013. The second method measured the concentration of cAMP in HEK-293 cell lysates treated for 30 minutes with saturating isoproterenol (10 $\mu$ M) using a cAMP enzyme immunoassay kit (ENZO life sciences) per mg protein, quantified by Coomassie protein assay (Thermo scientific). To assay for cAMP produced from endocytosed receptors, cells were pre-treated in serum-free media for 15 minutes with either 30 $\mu$ M Dyno-4a (Abcam) to block endocytosis or 0.1% DMSO (Sigma-Aldrich). The 5 maximum cAMP luminescence values were averaged for each condition, and reported as percent change of Dyno-4a treated compared to DMSO-treated.

### **Statistical analysis**

Results are displayed as mean of results from each experiment or data set, as indicated in figure legends. The statistical significance between conditions for experiments with two conditions was calculated using paired, two tailed t-tests. For experiments with  $\geq 3$  conditions, statistical significance was calculated using either Tukey or Dunnett's multiple comparison test, depending on experimental setup, following ordinary one-way ANOVA. For time course experiments, statistical significance was calculated using Dunnett's multiple comparison test following two-way ANOVA. All statistical calculations were performed using Prism6.0 software (GraphPad

Software, Inc). The threshold for significance was  $p < 0.05$  and the coding for significance is reported is: (ns)  $p > 0.05$ , (\*)  $p \leq 0.05$ , (\*\*)  $p \leq 0.01$ , (\*\*\*)  $p \leq 0.001$ , (\*\*\*\*)  $p \leq 0.00001$ .

## 2.7 References

Anon, ADRB2. *The Human Protein Atlas*. Available at:

<http://www.proteinatlas.org/ENSG00000169252-ADRB2/tissue> [Accessed June 1, 2016a].

Anon, Wls. *The Human Protein Atlas*. Available at:

<http://www.proteinatlas.org/ENSG00000116729-WLS/tissue>.

Belenkaya, T.Y. et al., 2008. The retromer complex influences Wnt secretion by recycling wntless from endosomes to the trans-Golgi network. *Developmental cell*, 14(1), pp.120–131.

Cao, T.T. et al., 1999. A kinase-regulated PDZ-domain interaction controls endocytic sorting of the beta2-adrenergic receptor. *Nature*, 401(6750), pp.286–290.

Cao, T.T., Brelot, A. & von Zastrow, M., 2005. The composition of the beta-2 adrenergic receptor oligomer affects its membrane trafficking after ligand-induced endocytosis. *Molecular pharmacology*, 67(1), pp.288–297.

Chen, D. et al., 2010. Retromer is required for apoptotic cell clearance by phagocytic receptor recycling. *Science*, 327(5970), pp.1261–1264.

Choy, R.W.-Y. et al., 2014. Retromer Mediates a Discrete Route of Local Membrane Delivery to Dendrites. *Neuron*, 82(1), pp.55–62.

Franch-Marro, X. et al., 2008. Wingless secretion requires endosome-to-Golgi retrieval

of Wntless/Evi/Sprinter by the retromer complex. *Nature cell biology*, 10(2), pp.170–177.

Gallon, M. et al., 2014. A unique PDZ domain and arrestin-like fold interaction reveals mechanistic details of endocytic recycling by SNX27-retromer. *Proceedings of the National Academy of Sciences of the United States of America*, 111(35), pp.E3604–13.

Gallon, M. & Cullen, P.J., 2015. Retromer and sorting nexins in endosomal sorting. *Biochemical Society transactions*, 43(1), pp.33–47.

Gasnereau, I. et al., 2011. Identification of an endocytosis motif in an intracellular loop of Wntless protein, essential for its recycling and the control of Wnt protein signaling. *The Journal of biological chemistry*, 286(50), pp.43324–43333.

Geuze, H.J. et al., 1984. Intracellular receptor sorting during endocytosis: comparative immunoelectron microscopy of multiple receptors in rat liver. *Cell*, 37(1), pp.195–204.

Gustafsson, M.G.L. et al., 2008. Three-Dimensional Resolution Doubling in Wide-Field Fluorescence Microscopy by Structured Illumination. *Biophysical journal*, 94(12), pp.4957–4970.

Haft, C.R. et al., 2000. Human Orthologs of Yeast Vacuolar Protein Sorting Proteins Vps26, 29, and 35: Assembly into Multimeric Complexes. *Molecular biology of the*



*cell*, 11(12), pp.4105–4116.

Haft, C.R. et al., 1998. Identification of a family of sorting nexin molecules and characterization of their association with receptors. *Molecular and cellular biology*, 18(12), pp.7278–7287.

Harterink, M. et al., 2011. A SNX3-dependent retromer pathway mediates retrograde transport of the Wnt sorting receptor Wntless and is required for Wnt secretion. *Nature cell biology*, 13(8), pp.914–923.

Horazdovsky, B.F. et al., 1997. A sorting nexin-1 homologue, Vps5p, forms a complex with Vps17p and is required for recycling the vacuolar protein-sorting receptor. *Molecular biology of the cell*, 8(8), pp.1529–1541.

Irannejad, R. et al., 2013. Conformational biosensors reveal GPCR signalling from endosomes. *Nature*, 495(7442), pp.534–538.

Lauffer, B.E.L. et al., 2010. SNX27 mediates PDZ-directed sorting from endosomes to the plasma membrane. *The Journal of cell biology*, 190(4), pp.565–574.

Lee, S., Chang, J. & Blackstone, C., 2016. FAM21 directs SNX27-retromer cargoes to the plasma membrane by preventing transport to the Golgi apparatus. *Nature communications*, 7, p.10939.

Masibay, A.S. et al., 1993. Mutational analysis of the Golgi retention signal of bovine beta-1,4-galactosyltransferase. *The Journal of biological chemistry*, 268(13),

pp.9908–9916.

Miesenböck, G., De Angelis, D.A. & Rothman, J.E., 1998. Visualizing secretion and synaptic transmission with pH-sensitive green fluorescent proteins. *Nature*, 394(6689), pp.192–195.

Nothwehr, S.F., S.-A., H. & Bruinsma, P., 2000. Sorting of Yeast Membrane Proteins into an Endosome-to-Golgi Pathway Involves Direct Interaction of Their Cytosolic Domains with Vps35p. *The Journal of cell biology*, 151(2), pp.297–310.

Pan, C.-L. et al., 2008. C. elegans AP-2 and retromer control Wnt signaling by regulating mig-14/Wntless. *Developmental cell*, 14(1), pp.132–139.

Port, F. et al., 2008. Wingless secretion promotes and requires retromer-dependent cycling of Wntless. *Nature cell biology*, 10(2), pp.178–185.

Puthenveedu, M.A. et al., 2010. Sequence-dependent sorting of recycling proteins by actin-stabilized endosomal microdomains. *Cell*, 143(5), pp.761–773.

Rasmussen, S.G.F., DeVree, B.T., et al., 2011. Crystal structure of the  $\beta$ 2 adrenergic receptor–Gs protein complex. *Nature*, 477(7366), pp.549–555.

Rasmussen, S.G.F., Choi, H.-J., et al., 2011. Structure of a nanobody-stabilized active state of the  $\beta$ (2) adrenoceptor. *Nature*, 469(7329), pp.175–180.

Rojas, R. et al., 2007. Interchangeable but essential functions of SNX1 and SNX2 in the association of retromer with endosomes and the trafficking of mannose

- 6-phosphate receptors. *Molecular and cellular biology*, 27(3), pp.1112–1124.
- Sankaranarayanan, S. et al., 2000. The use of pHluorins for optical measurements of presynaptic activity. *Biophysical journal*, 79(4), pp.2199–2208.
- Seaman, M.N. et al., 1997. Endosome to Golgi retrieval of the vacuolar protein sorting receptor, Vps10p, requires the function of the VPS29, VPS30, and VPS35 gene products. *The Journal of cell biology*, 137(1), pp.79–92.
- Seaman, M.N.J., 2007. Identification of a novel conserved sorting motif required for retromer-mediated endosome-to-TGN retrieval. *Journal of cell science*, 120(Pt 14), pp.2378–2389.
- Seaman, M.N., McCaffery, J.M. & Emr, S.D., 1998. A membrane coat complex essential for endosome-to-Golgi retrograde transport in yeast. *The Journal of cell biology*, 142(3), pp.665–681.
- Sharpe, H.J., Stevens, T.J. & Munro, S., 2010. A comprehensive comparison of transmembrane domains reveals organelle-specific properties. *Cell*, 142(1), pp.158–169.
- Snider, M.D. & Rogers, O.C., 1985. Intracellular movement of cell surface receptors after endocytosis: resialylation of asialo-transferrin receptor in human erythroleukemia cells. *The Journal of cell biology*, 100(3), pp.826–834.
- Swarbrick, J.D. et al., 2011. VPS29 is not an active metallo-phosphatase but is a rigid

scaffold required for retromer interaction with accessory proteins. *PloS one*, 6(5), p.e20420.

Tabuchi, M. et al., 2010. Retromer-mediated direct sorting is required for proper endosomal recycling of the mammalian iron transporter DMT1. *Journal of cell science*, 123(Pt 5), pp.756–766.

Tang, Y. et al., 1999. Identification of the endophilins (SH3p4/p8/p13) as novel binding partners for the beta 1-adrenergic receptor. *Proceedings of the National Academy of Sciences*, 96(22), pp.12559–12564.

Temkin, P. et al., 2011. SNX27 mediates retromer tubule entry and endosome-to-plasma membrane trafficking of signalling receptors. *Nature cell biology*, 13(6), pp.717–723.

Trousdale, C., Christopher, T. & Kyoungtae, K., 2015. Retromer: Structure, function, and roles in mammalian disease. *European journal of cell biology*, 94(11), pp.513–521.

Tsvetanova, N.G. & von Zastrow, M., 2014. Spatial encoding of cyclic AMP signaling specificity by GPCR endocytosis. *Nature chemical biology*, 10(12), pp.1061–1065.

Violin, J.D. et al., 2008. beta2-adrenergic receptor signaling and desensitization elucidated by quantitative modeling of real time cAMP dynamics. *The Journal of biological chemistry*, 283(5), pp.2949–2961.

- Wassmer, T. et al., 2007. A loss-of-function screen reveals SNX5 and SNX6 as potential components of the mammalian retromer. *Journal of cell science*, 120(Pt 1), pp.45–54.
- Yang, P.-T. et al., 2008. Wnt signaling requires retromer-dependent recycling of MIG-14/Wntless in Wnt-producing cells. *Developmental cell*, 14(1), pp.140–147.
- Yudowski, G.A., Puthenveedu, M.A. & von Zastrow, M., 2006. Distinct modes of regulated receptor insertion to the somatodendritic plasma membrane. *Nature neuroscience*, 9(5), pp.622–627.
- Yu, J. et al., 2014. WLS retrograde transport to the endoplasmic reticulum during Wnt secretion. *Developmental cell*, 29(3), pp.277–291.
- von Zastrow, M. & Kobilka, B.K., 1992. Ligand-regulated internalization and recycling of human beta 2-adrenergic receptors between the plasma membrane and endosomes containing transferrin receptors. *The Journal of biological chemistry*, 267(5), pp.3530–3538.
- Zhang, P. et al., 2011. SNX3 controls Wingless/Wnt secretion through regulating retromer-dependent recycling of Wntless. *Cell research*, 21(12), pp.1677–1690.

## 2.8 Figures

### **Figure 1. Direct comparison of retromer-dependent recycling and retrograde transport cargos in the same cells.**

(A) Schematic representation of Flag- $\beta$ 2AR (left) and HA-Wls (right) showing topology and epitope tagging. (B) Representative widefield images of HeLa cells expressing HA-Wls, stained without (top) or with (bottom) permeabilization. (C) Average Flag- $\beta$ 2AR and HA-Wls surface fluorescence upon control or VPS35 knockdown, as percent of control surface expression measured by fluorescence flow cytometry ( $n=3$  independent experiments). Error bars represent s.e.m. (D) Representative confocal images of permeabilized HEK-293 cells with no treatment (top) or with 30 minutes of saturating ( $10\mu\text{M}$ ) isoproterenol treatment (bottom), showing the localization of Flag- $\beta$ 2AR and HA-Wls. (E) Representative confocal images of HeLa cells expressing Flag- $\beta$ 2AR and HA-Wls, surface labeled with anti-Flag and -HA antibodies, and fixed after 0-minute (top) or 60-minute (bottom) chase incubation. Scale Bars,  $10\mu\text{m}$ . See also Figures S1 and S2.

### **Figure 2. $\beta$ 2AR and Wls traffic through the same endosomes and retromer endosome domains.**

(A) Representative confocal image of a HeLa cell expressing Flag- $\beta$ 2AR and HA-Wls surface labeled with anti-Flag and HA antibodies and fixed after 15-minute chase incubation. Inset shows a representative region at higher magnification. (B) Representative confocal image of live a HEK-293 cell expressing Flag- $\beta$ 2AR, HA-Wls,

and VPS29-mCherry surface labeled with anti-Flag and HA antibodies after chase incubation. Inset shows a representative region at higher magnification. **(C)** Enlarged view of an endosome in a HEK-293 cell with a RED (arrows) containing both Flag- $\beta$ 2AR and HA-Wls. **(D)** Quantification of cargos in REDs after 7-51 minute chase incubations ( $n=3$  independent experiments). Error bars correspond to s.e.m. Large image scale bars, 10 $\mu$ m; inset scale bars, 1 $\mu$ m.

**Figure 3.  $\beta$ 2AR and Wls have distinct abilities to enrich in and exit from REDs.**

**(A)** Representative confocal image of an endosome in a HEK-293 cell surface labeled for Flag- $\beta$ 2AR and HA-Wls. Dotted line in merge panel shows line used for fluorescence intensity profile in B. **(B)** Fluorescence intensity profile, normalized to maximum, of line shown in panel A. **(C)** Average RED enrichment indices of Flag- $\beta$ 2AR and HA-Wls, defined as the ratio of the mean, background-subtracted fluorescence per pixel in the RED divided by the mean, background-subtracted fluorescence per pixel in the adjacent endosome ( $n=30$  REDs pooled from 3 independent experiments). Inset image shows an example of the regions of interest used to quantify the endosome (dotted circle) and RED (dotted curved line). **(D)** Representative time-lapse series of a RED scission event, with relative time in seconds denoted to left of each image. Dotted lines in merge image panels show lines used for fluorescence intensity profiles in E. **(E)** Fluorescence intensity profiles, normalized to series maximum, of lines shown in panel D. **(F)** Average exiting vesicle to endosome ratios of Flag- $\beta$ 2AR and HA-Wls, defined as the ratio of the mean, background-subtracted exiting vesicle fluorescence per pixel divided by the

mean, background-subtracted endosome fluorescence per pixel ( $n=24$  events pooled from 3 independent experiments). Inset image show an example of the regions of interest used for the endosome (large dotted shape) and RED (small dotted shape). Error bars correspond to s.e.m. Scale bars, 1 $\mu$ m. See also Figure S3.

**Figure 4. Identification of  $\Phi$ -X-[L/M] motifs in Wls' cytoplasmic tail required for strong RED enrichment and retrograde transport.**

**(A-C)** Left, schematic representations of HA-Wls wild type, HA-Wls $\Delta$ 35, and HA-Wls(LQL+YKL>AAA) showing the corresponding mutations, topology, and epitope tagging. Center, representative confocal images of live HEK-293 cells surface labeled for HA-Wls wild type, HA-Wls $\Delta$ 35, or HA-Wls(LQL+YKL>AAA) and Flag- $\beta$ 2AR after chase incubations. Inset images show representative endosomes with REDs at higher magnification. Right, average RED enrichment indices of HA-Wls wild type, HA-Wls $\Delta$ 35, and HA-Wls(LQL+YKL>AAA) compared to Flag- $\beta$ 2AR in the same REDs ( $n=30$  REDs pooled from 3 independent experiments). **(D)** Amino acid sequence alignment of the cytoplasmic tails of Wls from different species with  $\Phi$ -X-[L/M] motifs highlighted in cyan and putative [S/T]-X-[L/M] motifs highlighted in purple. **(E-G)** Representative confocal images of fixed HeLa cells expressing HA-Wls wild type, HA-Wls $\Delta$ 35, or HA-Wls(LQL+YKL>AAA) surface labeled with anti-HA antibodies and chased for 60 minutes. **(H)** Accumulation of each cargo in the TGN, quantified by average Pearson's correlation coefficient with TGN46 after a 60-minute chase incubation ( $n=30$  cells



pooled from 3 independent experiments). Large image scale bars, 10 $\mu$ m; inset scale bars, 1 $\mu$ m. Error bars correspond to s.e.m. See also Figure S4.

**Figure 5. Wls' and  $\beta$ 2AR's cytoplasmic tails determine RED enrichment and trafficking kinetics, but not target destination.**

(A, B) Left, schematic representations of Flag- $\beta$ 2AR wild type or Flag- $\beta$ 2AR $\Delta$ 42-Wls35 showing corresponding mutations, topology, and epitope tagging. Center, representative confocal images of live HEK-293 cells surface labeled for Flag- $\beta$ 2AR wild type or Flag- $\beta$ 2AR $\Delta$ 42-Wls35 and HA- $\beta$ 2AR after chase incubations. Inset images show representative endosomes with REDs at higher magnification. Right, average RED enrichment indices of Flag- $\beta$ 2AR wild type or Flag- $\beta$ 2AR $\Delta$ 42-Wls35 compared to HA- $\beta$ 2AR in the same REDs ( $n=30$  REDs pooled from 3 independent experiments). (C) Average percent recycled Flag- $\beta$ 2AR wild type or mutant after 45 minutes of agonist washout ( $n=5$ ). (D) Average percent recycled Flag- $\beta$ 2AR wild type or mutant after denoted time points of agonist washout, with statistical significance shown in relation to wild type Flag- $\beta$ 2AR ( $n=4$ ). (E, F) Left, schematic representations of HA-Wls wild type or HA-Wls $\Delta$ 35- $\beta$ 2AR42 showing corresponding mutations, topology, and epitope tagging. Center, representative confocal images of live HEK-293 cells surface labeled for HA-Wls wild type or HA-Wls $\Delta$ 35- $\beta$ 2AR42 and Flag- $\beta$ 2AR after chase incubation. Inset images show representative endosomes with REDs at higher magnification. Right, average RED enrichment indices of HA-Wls wild type or HA-Wls $\Delta$ 35- $\beta$ 2AR42 compared to Flag- $\beta$ 2AR in the same REDs ( $n=30$  REDs pooled from 3 independent

experiments). **(G)** Average Pearson's correlation coefficient of each cargo with TGN46 after 60-minute chase incubation, indicating accumulation of each cargo in the TGN ( $n=30$  cells pooled from 3 independent experiments). **(H)** Average Pearson's correlation coefficient of each cargo with TGN46 after denoted time points of chase incubation, with statistical significance shown in relation to wild type HA-Wls ( $n=30$  cells pooled from 3 independent experiments). Large image scale bars, 10 $\mu$ m; inset scale bars, 1 $\mu$ m. Error bars correspond to s.e.m. See also Figure S5.

**Figure 6.  $\beta$ 2AR and Wls are each able to transit both the plasma membrane and the TGN.**

**(A)** Left, representative TIR-FM image montage showing coincident plasma membrane insertion of Sph-B2AR and surface labeled Flag in a live HEK-293 expressing Flag-SpH- $\beta$ 2AR. Right, fluorescence traces showing that surface labeled Flag appears in the TIRF field prior to SpH insertion and that both signals rapidly diffuse. **(B)** Left, representative TIR-FM image montage showing coincident plasma membrane insertion of Sph-Wls and surface labeled HA in a live HEK-293 expressing HA-SpH-Wls. Right, fluorescence traces showing that surface labeled HA appears in the TIRF field prior to SpH insertion and that both signals rapidly diffuse. **(C)** Average  $\Delta F/F_0$  plot of SpH signals of insertion events from cells expressing either SpH-Flag- $\beta$ 2AR or SpH-HA-Wls ( $n=10$  events from two independent experiments). **(D)** Representative TIR-FM image montage showing coincident plasma membrane insertion of Sph and surface labeled Flag (arrows) in a live HEK-293 expressing both HA-SpH-Wls and Flag- $\beta$ 2AR. Right,

fluorescence traces showing that surface labeled Flag appears in the TIRF field prior to SpH insertion and that both signals rapidly diffuse. **(E)** Representative immunoblots of cell lysates upon control or FAM21 siRNA knockdown blotted for FAM21 or GAPDH. Average percent knockdown upon treatment with FAM21 siRNA was quantified at  $83.0 \pm 13.6\%$  of control (mean  $\pm$  standard deviation,  $n=3$ ). **(F)** Representative confocal images of fixed HeLa cells expressing Flag- $\beta$ 2AR, treated with control or FAM21 siRNA, and surface labeled with anti-Flag antibody, chased for 60 minutes. **(G)** Representative confocal images of fixed HeLa cells expressing HA-Wls, treated with control or FAM21 siRNA, and surface labeled with anti-Flag antibody, chased for 60 minutes. **(H)** Accumulation of each cargo in the TGN upon control or FAM21 knockdown, quantified by average Pearson's correlation coefficient with TGN46 after a 60-minute chase incubation ( $n=30$  cells pooled from 3 independent experiments). **(I)** Representative confocal images of live HEK-293 cells treated with either control or FAM21 siRNA surface labeled for HA-Wls and Flag- $\beta$ 2AR after chase incubation. Inset images show representative endosomes with REDs at higher magnification. Inset scale bar,  $1\mu\text{m}$ . **(J)** Average RED enrichment indices of Flag- $\beta$ 2AR and HA-Wls upon control or FAM21 knockdown ( $n=30$  REDs pooled from 3 independent experiments). **(K)** Representative confocal images of permeabilized HeLa cells expressing either HA-Wls or HA-Wls $\Delta$ 35 showing steady state localization relative to TGN46. **(L)** Average Pearson's correlation coefficient of HA-Wls and HA-Wls $\Delta$ 35 with TGN46 at steady state ( $n=20$  cells pooled from 2 independent experiments). Large image scale bars;  $10\mu\text{m}$ . TIR-FM montage scale bars,  $1\mu\text{m}$ . Error bars correspond to s.e.m.

**Figure 7.  $\beta$ 2AR mutant RED enrichment is inversely correlated with G protein activation at endosomes.**

**(A-C)** Left, schematic representations of Flag- $\beta$ 2AR $\Delta$ PDZ, Flag- $\beta$ 2AR wild-type, or Flag- $\beta$ 2AR $\Delta$ 42-Wls35 showing corresponding mutations, topology, and epitope tagging. Note that constructs are ordered by increasing RED enrichment from top to bottom. Right, representative confocal images of live HEK-293 cells expressing Flag- $\beta$ 2AR $\Delta$ PDZ, Flag- $\beta$ 2AR wild-type, or Flag- $\beta$ 2AR $\Delta$ 42-Wls35 and Nb80-GFP after Flag surface labeling and subsequent chase incubation. Inset images show representative endosomes at higher magnification. **(D)** Average Nb80-GFP to Flag fluorescence enrichment ratio in endosomes, ( $n=30$  cells from 3 independent experiments). **(E-G)** Representative confocal images of live HEK-293 cells expressing Flag- $\beta$ 2AR $\Delta$ PDZ, Flag- $\beta$ 2AR wild-type, or Flag- $\beta$ 2AR $\Delta$ 42-Wls35 and Nb37-GFP after surface Flag labeling and subsequent chase incubation. Inset images show representative endosomes at higher magnification. **(H)** Average Nb37-GFP to Flag fluorescence enrichment ratio in endosomes ( $n=30$  cells from 3 independent experiments). Large image scale bars, 10 $\mu$ m; inset scale bars, 1 $\mu$ m. Error bars correspond to s.e.m. **(I)** Schematic model summarizing key findings relating to sorting of  $\beta$ 2AR and Wls downstream of shared cargo exit from endosomes. Events depicted as numbered items in model correspond to those discussed in the text. **(J)** Schematic model summarizing key findings relating to retromer's regulation of kinetic sorting and  $\beta$ 2AR signal activation at the endosome. See also Figure S6.

**Supplemental Figure 1. Topology and localization of additional epitope-tagged WIs constructs. Related to Figure 1.**

(A) Schematic representation of HA-WIs-ERretrieval, which does not contain the C-terminal HA epitope to block the endogenous ER retrieval motif, showing topology and epitope tagging. (B) Representative epifluorescence images of fixed HEK-293 cells expressing HA-WIs-ER retrieval, without (top) or with (bottom) permeabilization, showing that the recombinant protein is not strongly localized to the plasma membrane and instead accumulates in a juxtannuclear region that does not colocalize with Golgi-resident protein Giantin, indicative of ER localization. (C) Schematic representation of Flag-WIs-HA showing topology and epitope tagging. (D) Representative epifluorescence images of fixed HEK-293 cells expressing Flag-WIs-HA, without (top) or with (bottom) permeabilization, showing that recombinant protein can be detected at the plasma membrane with only Flag antibody and that both epitopes colocalize almost perfectly at a perinuclear region, indicative of TGN localization.

**Supplemental Figure 2. Relative expression levels of epitope tagged  $\beta$ 2AR and WIs and assessment of co-expression on membrane trafficking. Related to Figure 1.**

(A) Relative surface expression of HA- $\beta$ 2AR and HA-WIs measured by fluorescence flow cytometry ( $n=3$  independent experiments). (B) Representative immunoblot showing relative levels of (1) Flag- $\beta$ 2AR to Flag-WIs and (2) Flag-WIs to endogenous WIs. HeLa

cells were transfected with constructs as indicated above each lane and cell lysates expressing both Flag-β2AR and Flag-Wls were loaded in a dilution series to quantify relative expression levels. Top image shows representative blot probed with anti-Flag antibody, showing relative protein expression of Flag-β2AR and Flag-Wls expression; relative expression was quantified at 6.5 Wls: 1 β2AR in this example and overexpression averaged  $12.5 \pm 5.1$  Wls: 1 β2AR ( $n=4$ ). Center image shows blot probed with anti-Wls antibody, showing relative protein expression of endogenous Wls and overexpressed Flag-Wls. Relative expression was quantified at 5.3 Flag-Wls: 1 endogenous Wls in this example and overexpression averaged  $4.3 \pm 1.8$  Flag-Wls: endogenous Wls ( $n=4$ ). Lower image shows blot probed with anti-GAPDH, showing relative loading. Molecular weights and corresponding epitope-tagged proteins are denoted on right. **(C)** Average percent recycled Flag-β2AR upon co-expression of either empty vector (pcDNA) or HA-Wls ( $n=3$ ). **(D)** Representative confocal images of fixed HeLa cells expressing HA-Wls and co-expressing either empty vector (pcDNA) or Flag-β2AR, surface labeled with anti-HA antibodies and chased for 60 minutes. Scale bar, 10um. **(E)** Accumulation of HA-Wls in the TGN when co-expressed with either empty vector (pcDNA) or Flag-β2AR after a 60-minute chase incubation ( $n=20$  cells from 2 independent experiments). Error bars represent s.e.m.

**Supplemental Figure 3. Structured illumination microscopy (SIM) confirms β2AR and Wls have distinct abilities to enrich in REDs. Related to Figure 3.**

(A) Representative SIM reconstruction images of a live HEK-293 cell expressing HA-Wls and Flag- $\beta$ 2AR and surface labeled with anti-Flag and HA antibodies after chase incubation. Inset images show representative endosomes at higher magnification. Large image scale bars, 10 $\mu$ m; inset scale bars, 1 $\mu$ m. (B) Average RED enrichment indices of Flag- $\beta$ 2AR and HA-Wls. ( $n=30$  REDs pooled from 2 independent experiments).

**Supplemental Figure 4. Bipartite nature of the retromer sorting determinant in the Wls cytoplasmic tail. Related to Figure 4.**

(A) Amino acid sequences of the cytoplasmic tails of: (i) wild type human  $\beta$ 2AR, (ii) wild type human Wls, (iii) Wls $\Delta$ 35, (iv) Wls $\Delta$ 518-541, (v) Wls $\Delta$ 506-518, and (vi) Wls(LQL+YKL>AAA). In the  $\beta$ 2AR sequence, the PDZ motif is underlined and in the Wls sequences, the  $\Phi$ -X-[L/M] motifs are in cyan. In the Wls(LQL+YKL>AAA) sequence, mutated residues are shown in grey. (B, C) Left, schematic representations of HA-Wls $\Delta$ 518-541 (B) and HA-Wls $\Delta$ 506-518 (C) showing topology, epitope tagging, and mutations. Center, representative confocal images of live HEK-293 cells expressing HA-Wls $\Delta$ 518-541 (B) or HA-Wls $\Delta$ 506-518 (C) and Flag- $\beta$ 2AR after surface Flag and HA labeling and subsequent chase incubations. Inset images show representative endosomes with REDs at higher magnification. Right, average RED enrichment indices of HA-Wls $\Delta$ 518-541 (B) or HA-Wls $\Delta$ 506-518 (C) compared to Flag- $\beta$ 2AR in the same REDs ( $n=30$  REDs pooled from 3 independent experiments). (D) Representative confocal images of HeLa cells expressing HA-Wls $\Delta$ 518-541 or HA-Wls $\Delta$ 506-518

surface labeled with anti-HA antibodies and chased for 60 minutes (**E**) Accumulation of each cargo in the TGN, quantified by average Pearson's correlation coefficient with TGN46 after a 60-minute chase incubation ( $n=30$  cells pooled from 3 independent experiments). Large image scale bars, 10 $\mu$ m; inset scale bars, 1 $\mu$ m. Error bars correspond to s.e.m.

**Supplemental Figure 5. Cytoplasmic tail swapping between  $\beta$ 2AR and WIs does not change downstream destination. Related to Figure 5.**

(**A**) Representative confocal images of fixed HeLa cells expressing Flag- $\beta$ 2AR, Flag- $\beta$ 2AR $\Delta$ 42, or Flag- $\beta$ 2AR $\Delta$ 42-WIs35 surface labeled with anti-Flag antibody and chased for 60 minutes. (**B**) Accumulation of each cargo in the TGN after 60-minute chase incubation, compared to HA-WIs, quantified by average Pearson's correlation coefficient with TGN46 ( $n=30$  cells pooled from 3 independent experiments). Error bars correspond to s.e.m. (**C**) Representative confocal images of fixed HeLa cells expressing HA-WIs, HA-WIs $\Delta$ 35, HA-WIs $\Delta$ 35- $\beta$ 2AR42, or HA- $\beta$ 2AR surface labeled with anti-HA antibodies and chase incubated for 60 minutes. Scale bars, 10 $\mu$ m.

**Supplemental Figure 6. B2AR mutant constructs are functional in signaling assays and do not significantly alter the fraction cAMP produced from endosomes. Related to Figure 7.**

(**A**) Isoproterenol-induced cAMP luminescence traces, normalized to forskolin maxima, from live HEK-293 cells stably expressing indicated constructs ( $n=2$ ). (**B**) Integrated



cAMP luminescence from plot shown in A. **(C)** Fold change of cAMP in cells stably expressing the indicated constructs lysed after 30 minutes of isoproterenol treatment compared to non-transfected cells measured by Elisa ( $n= 3$ ). **(D)** Left, schematic representations of Flag- $\beta 2AR\Delta 42$ -Wls35(LQL+YKL>AAA) showing corresponding mutations, topology, and epitope tagging. Right, representative confocal image of a live HEK-293 cell expressing Flag- $\beta 2AR\Delta 42$ -Wls35(LQL+YKL>AAA) and Nb37-GFP after Flag surface labeling and subsequent chase incubation. Inset images show representative endosome at higher magnification. Large image scale bar, 10 $\mu$ m; inset scale bar, 1 $\mu$ m. **(E)** Average Nb37-GFP to Flag fluorescence enrichment ratio in endosomes, ( $n=10$  cells from 1 experiment). **(F)** Percent inhibition of maximal isoproterenol-induced cAMP luminescence by endocytic inhibitor Dyngo-4a in cells stably expressing the indicated constructs ( $n=4$ ).

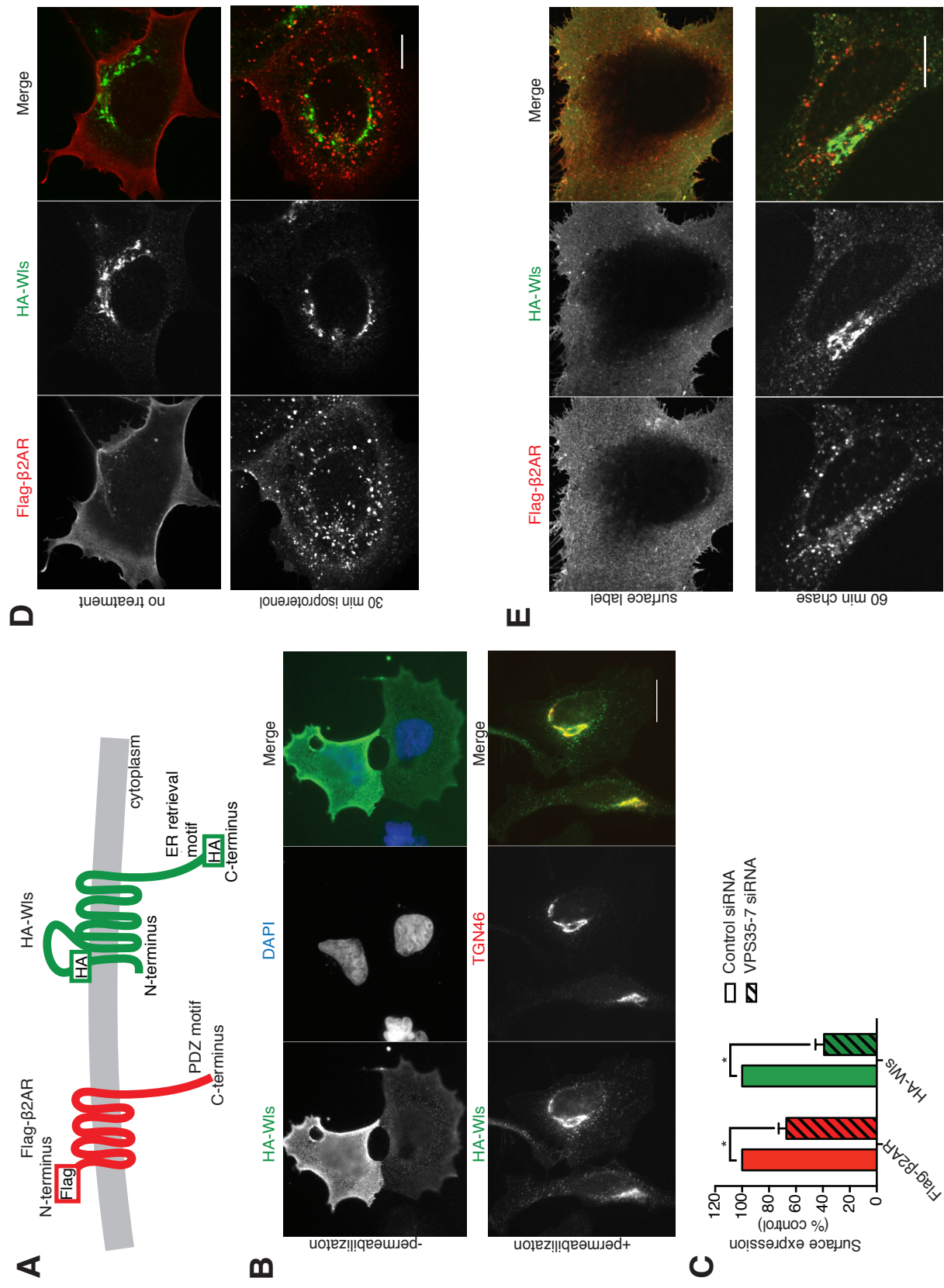


**Figure 1.** Direct comparison of retromer-dependent recycling and retrograde transport cargos in the same cells.

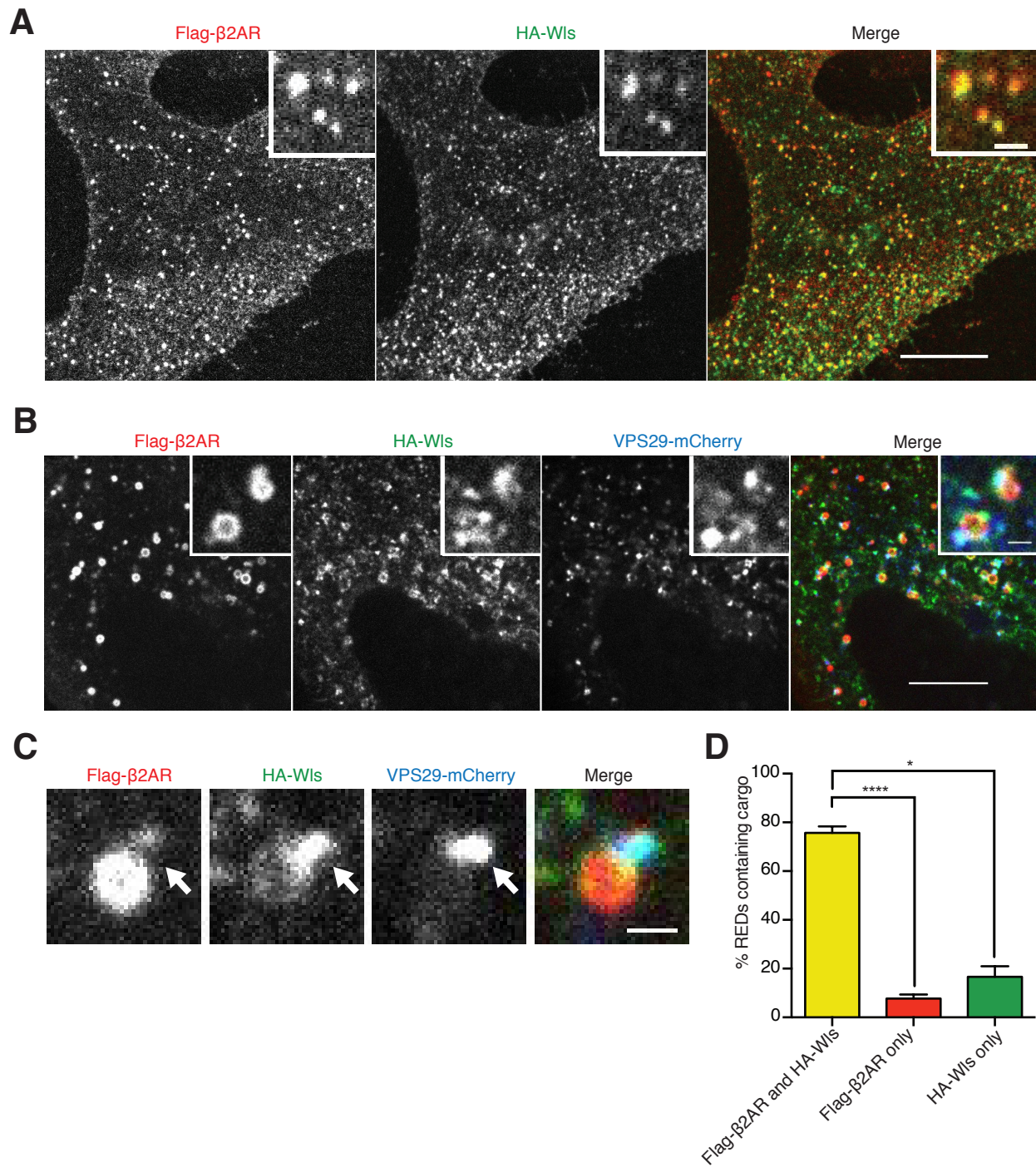


**Figure 2.**  $\beta$ 2AR and Wls traffic through the same endosomes and retromer endosome domains.

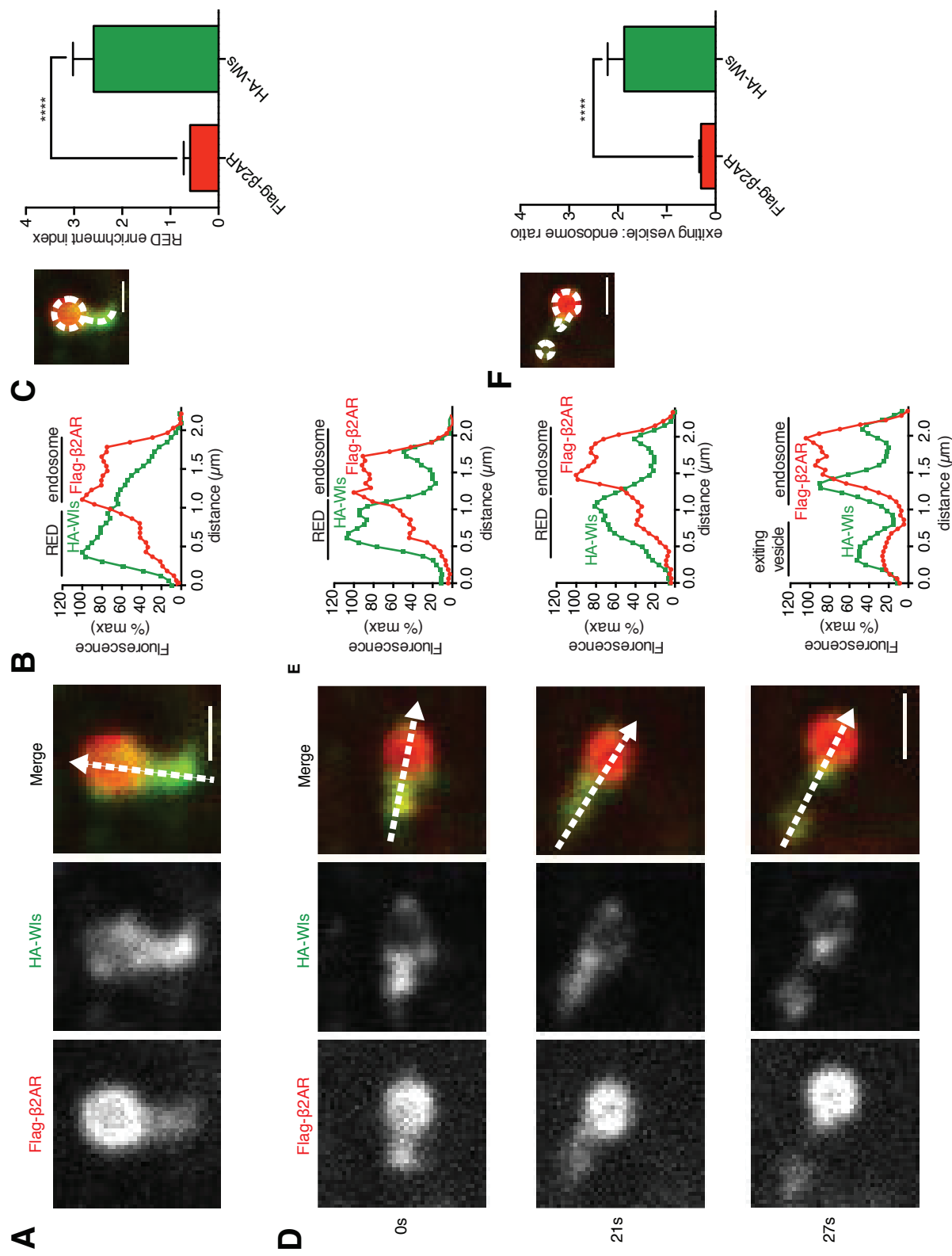


**Figure 3.**  $\beta$ 2AR and WIs have distinct abilities to enrich in and exit from REDs.



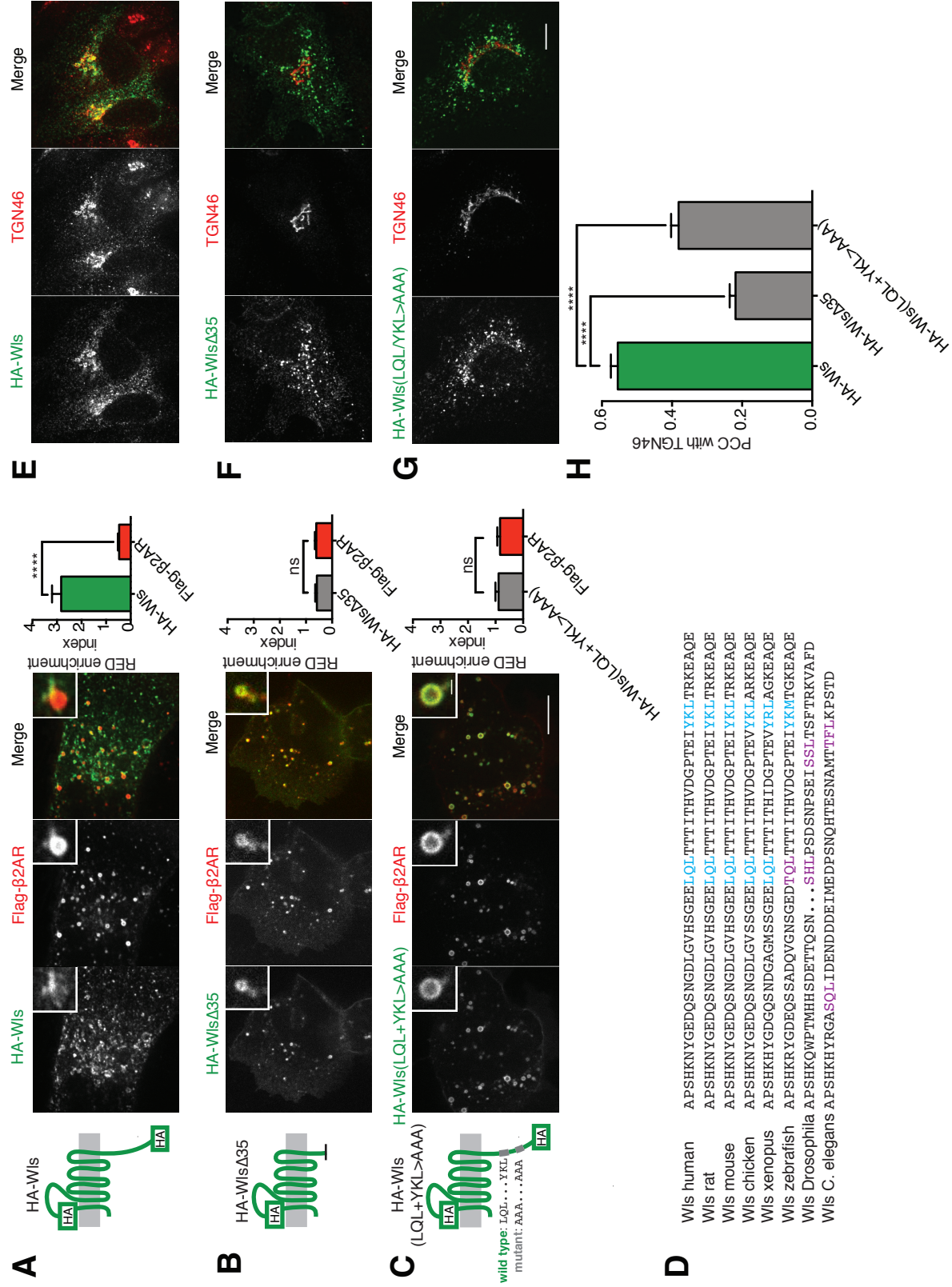


**Figure 4.** Identification of  $\Phi$ -X-[L/M] motifs in Wls' cytoplasmic tail required for strong RED enrichment and retrograde transport.

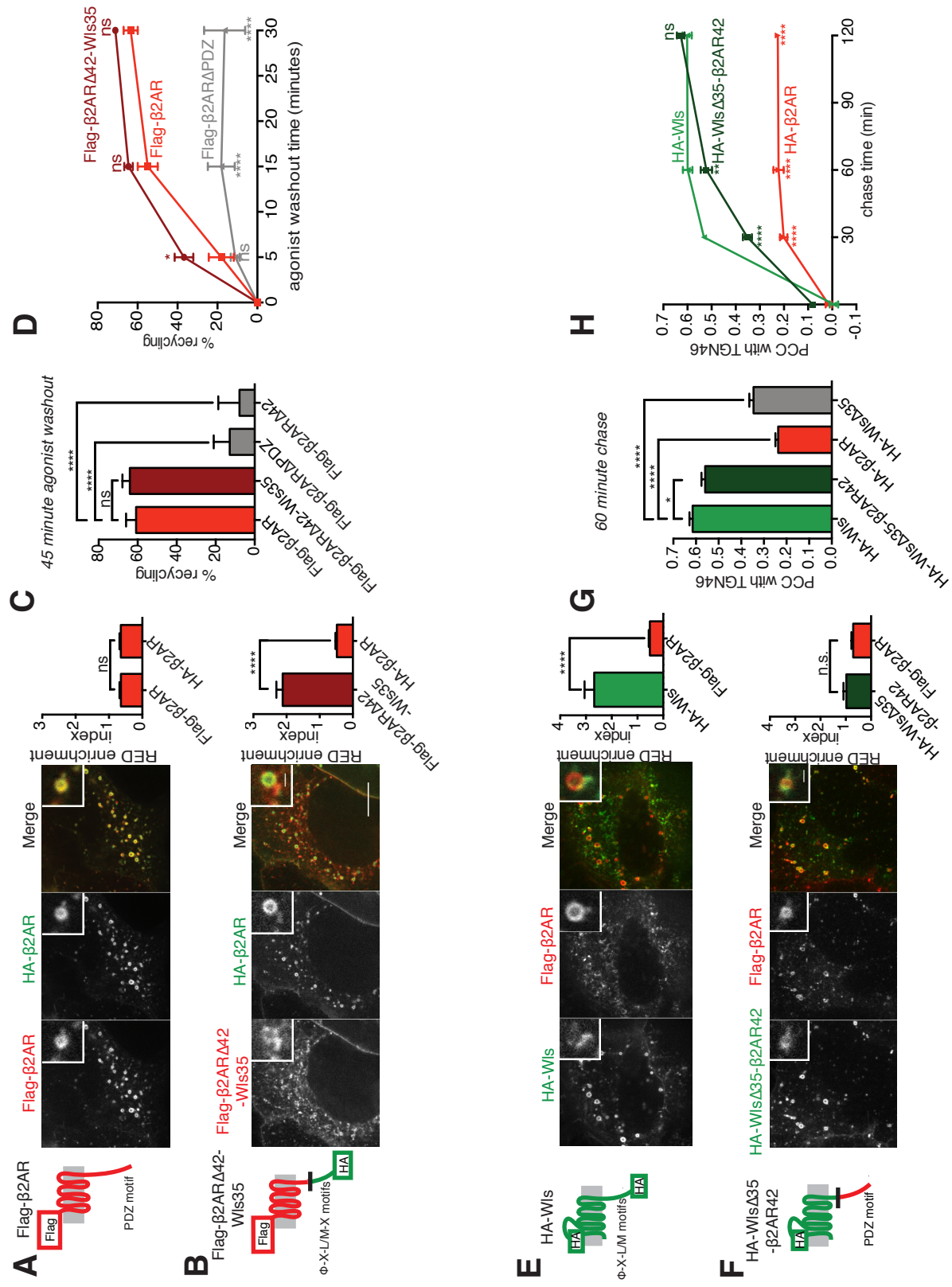


**Figure 5.** Wis' and β2AR's cytoplasmic tails determine RED enrichment and trafficking kinetics, but not target destination.

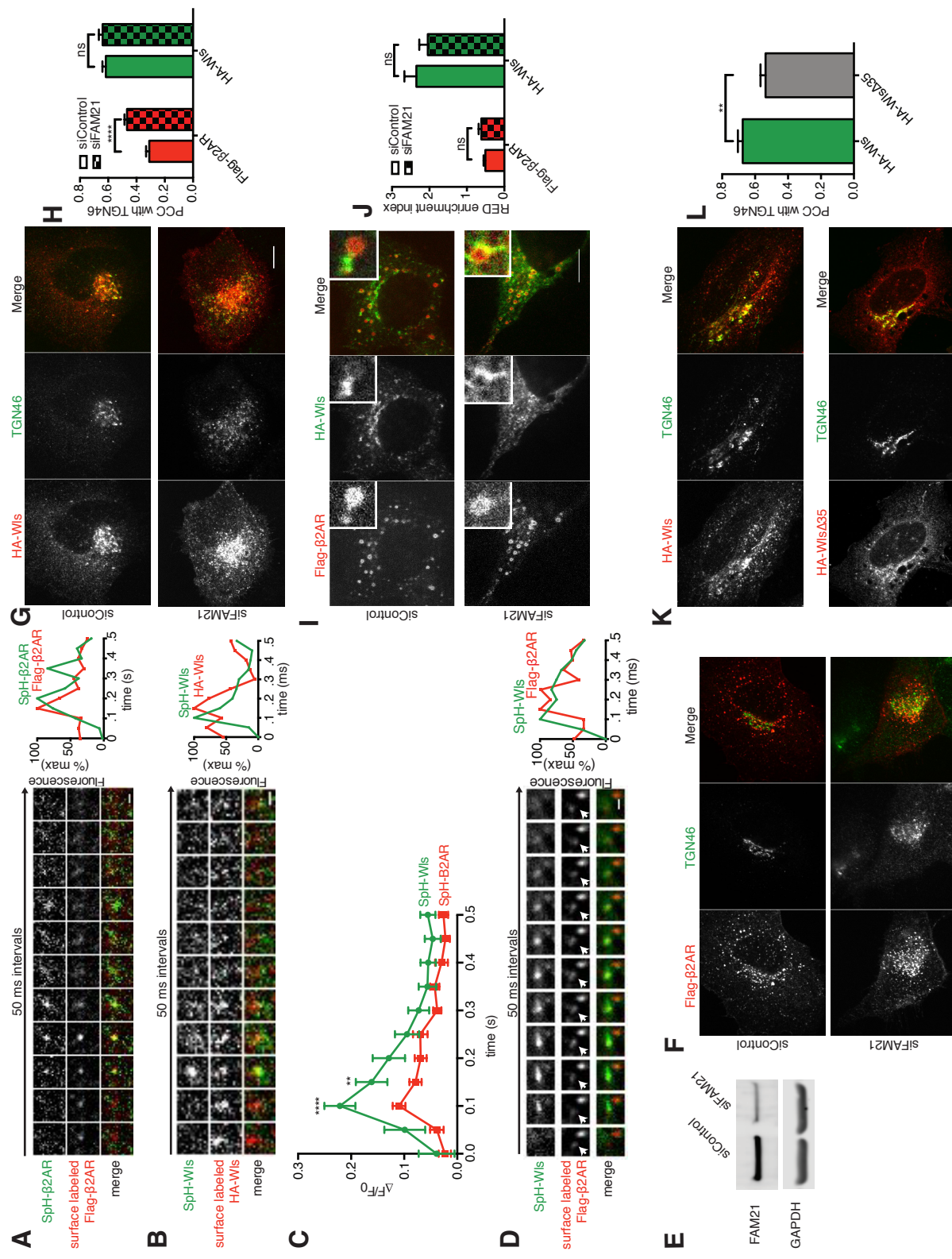


**Figure 6.**  $\beta$ 2AR and WIs are each able to transit both the plasma membrane and the TGN.



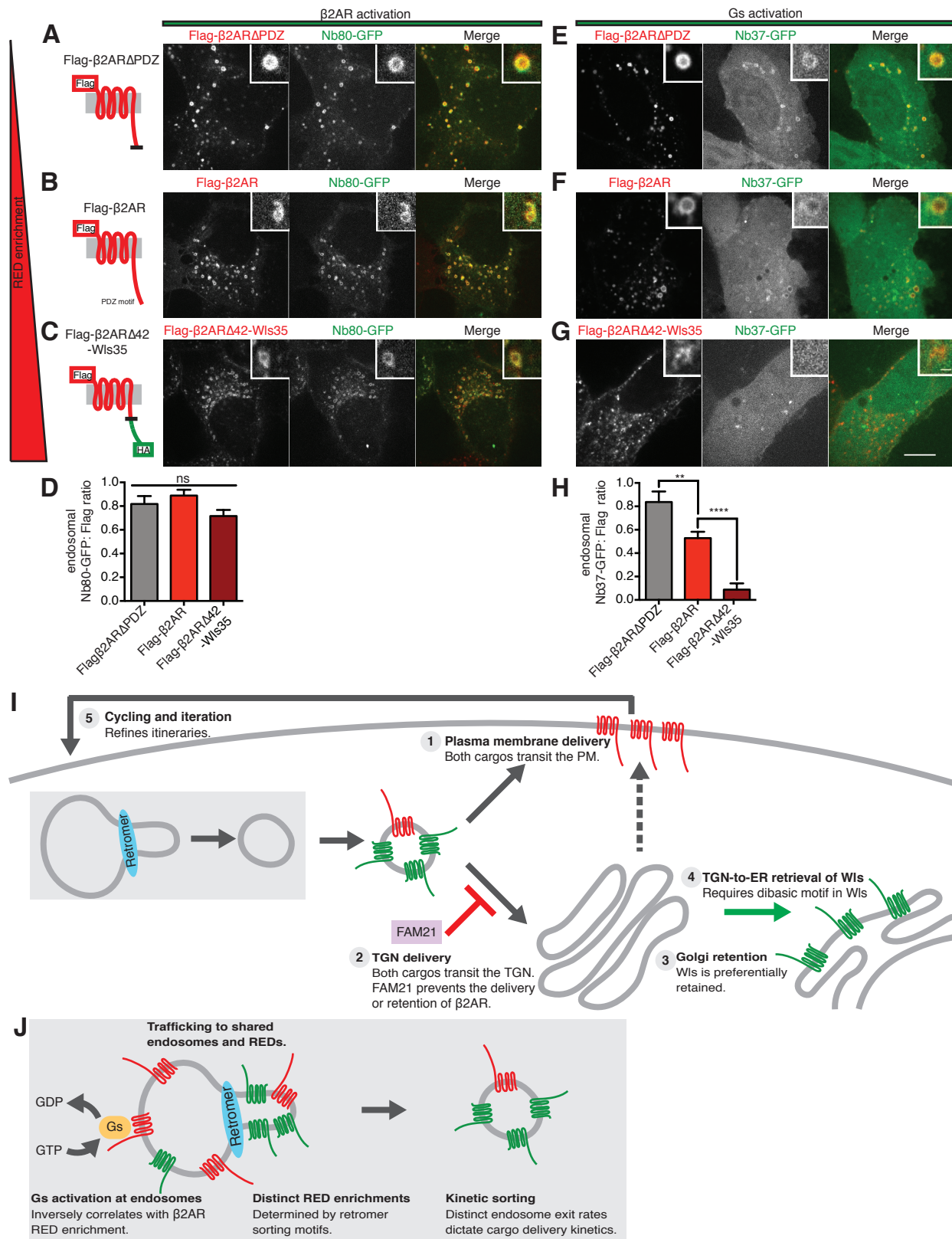


**Figure 7.**  $\beta$ 2AR mutant RED enrichment is inversely correlated with G protein activation at endosomes.



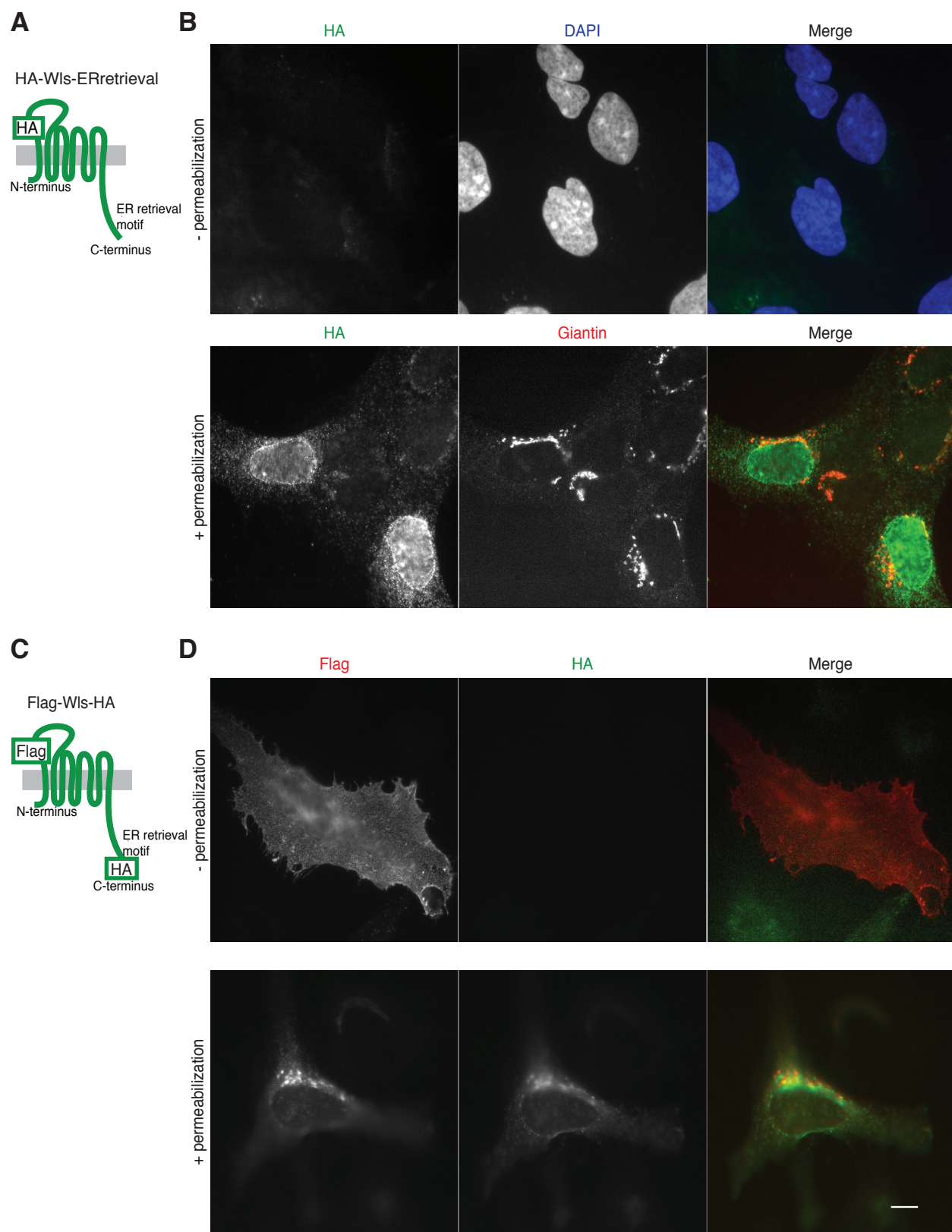


**Figure S1.** Topology and localization of additional epitope-tagged Wls constructs.

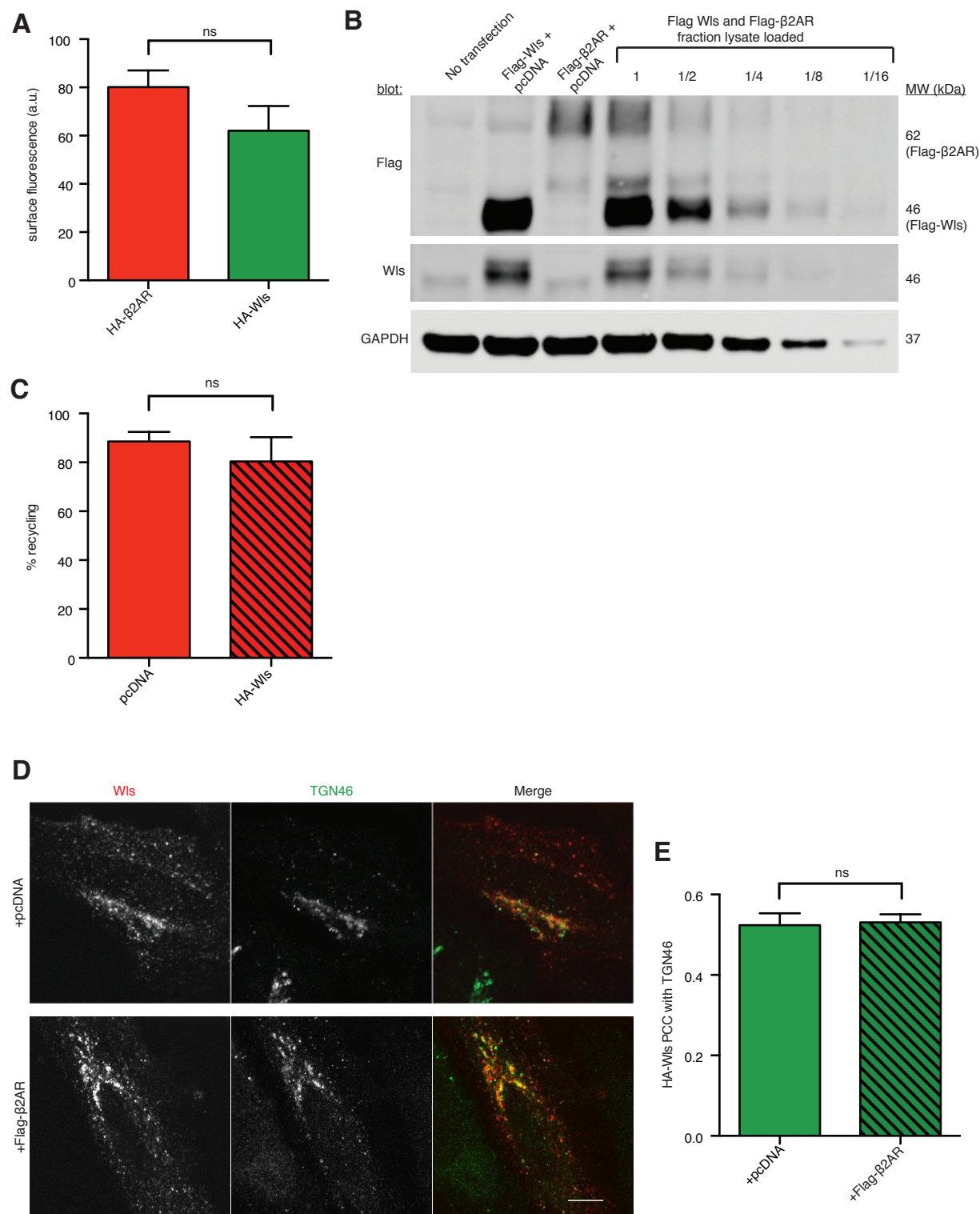


**Figure S2.** Relative expression levels of epitope tagged  $\beta$ 2AR and Wls and assessment of co-expression on membrane trafficking.

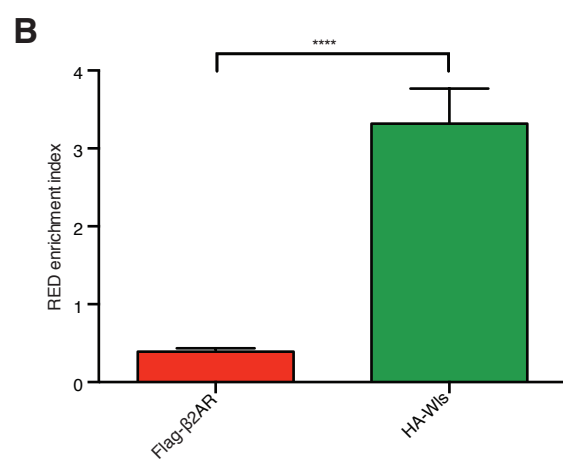
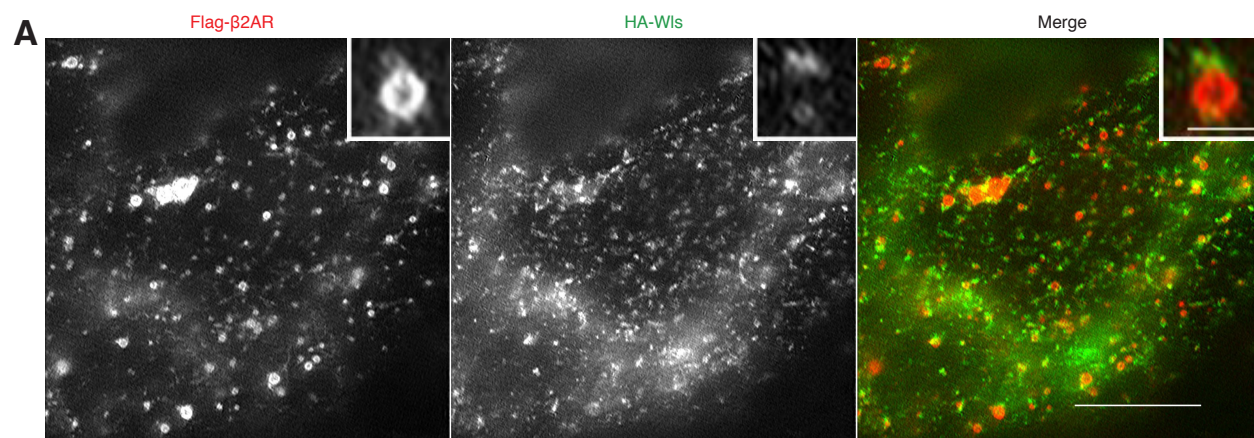


**Figure S3.** Structured illumination microscopy (SIM) confirms  $\beta$ 2AR and Wls have distinct abilities to enrich in REDs.



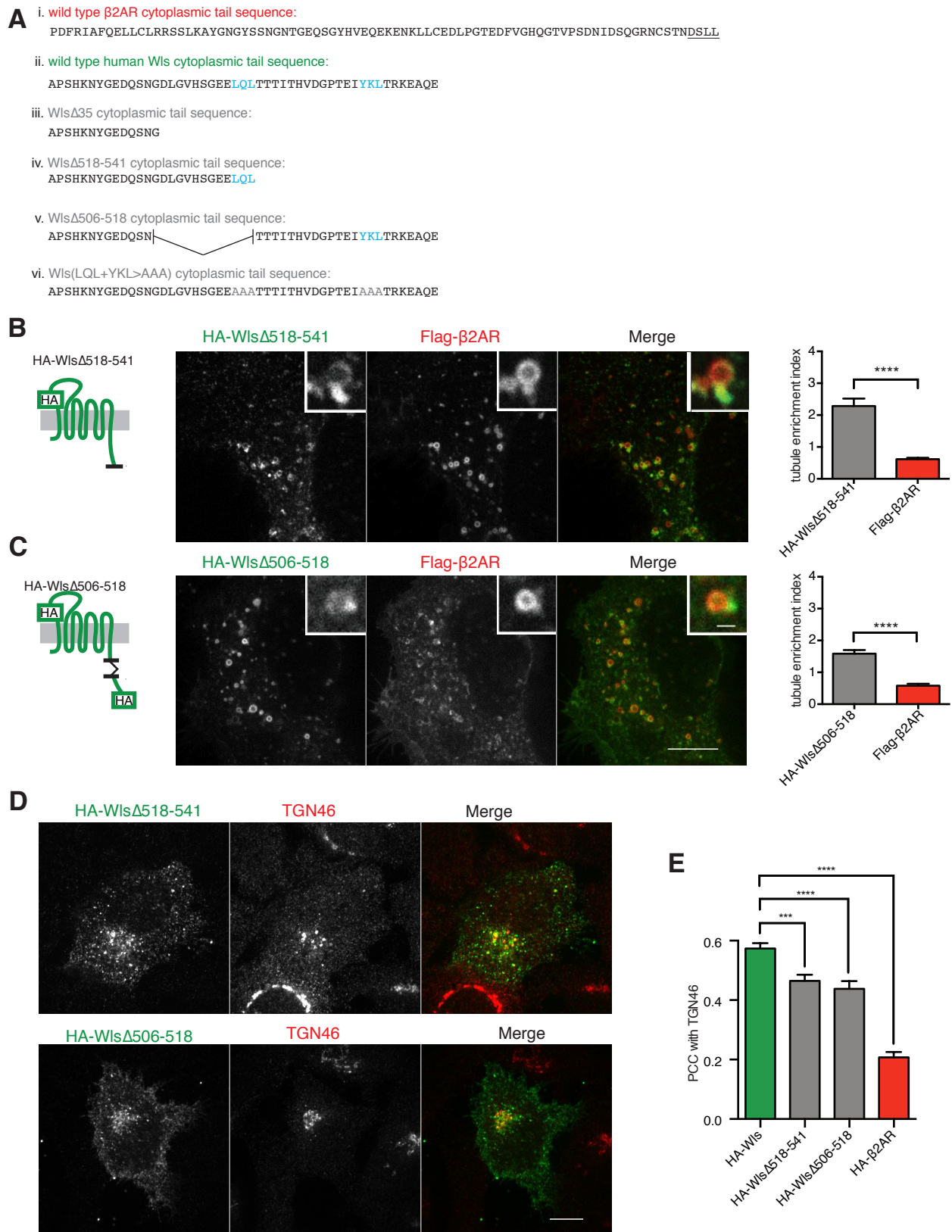


**Figure S4.** Bipartite nature of the retromer sorting determinant in the Wls cytoplasmic tail.

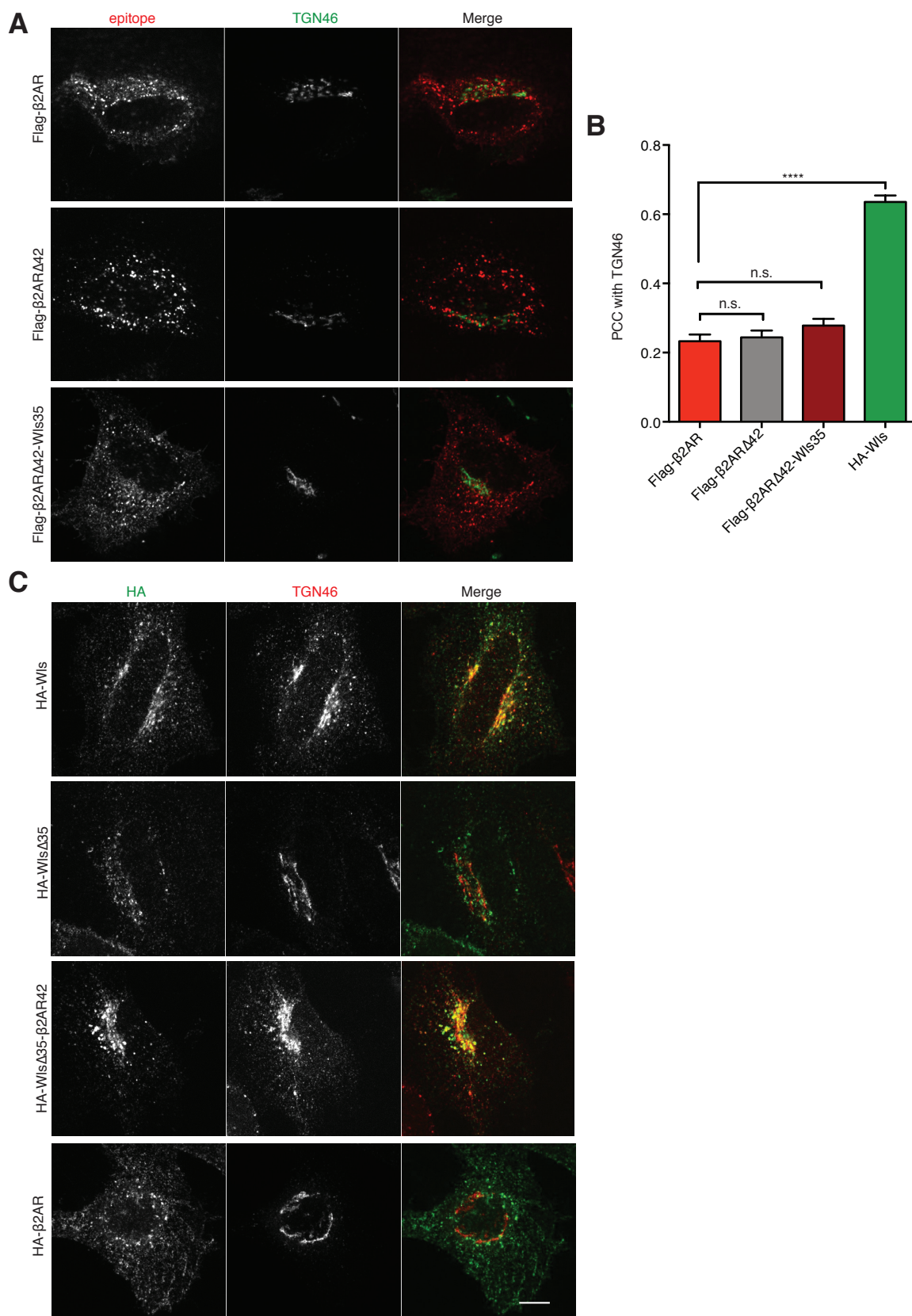


**Figure S5.** Cytoplasmic tail swapping between  $\beta$ 2AR and WIs does not change downstream destination.

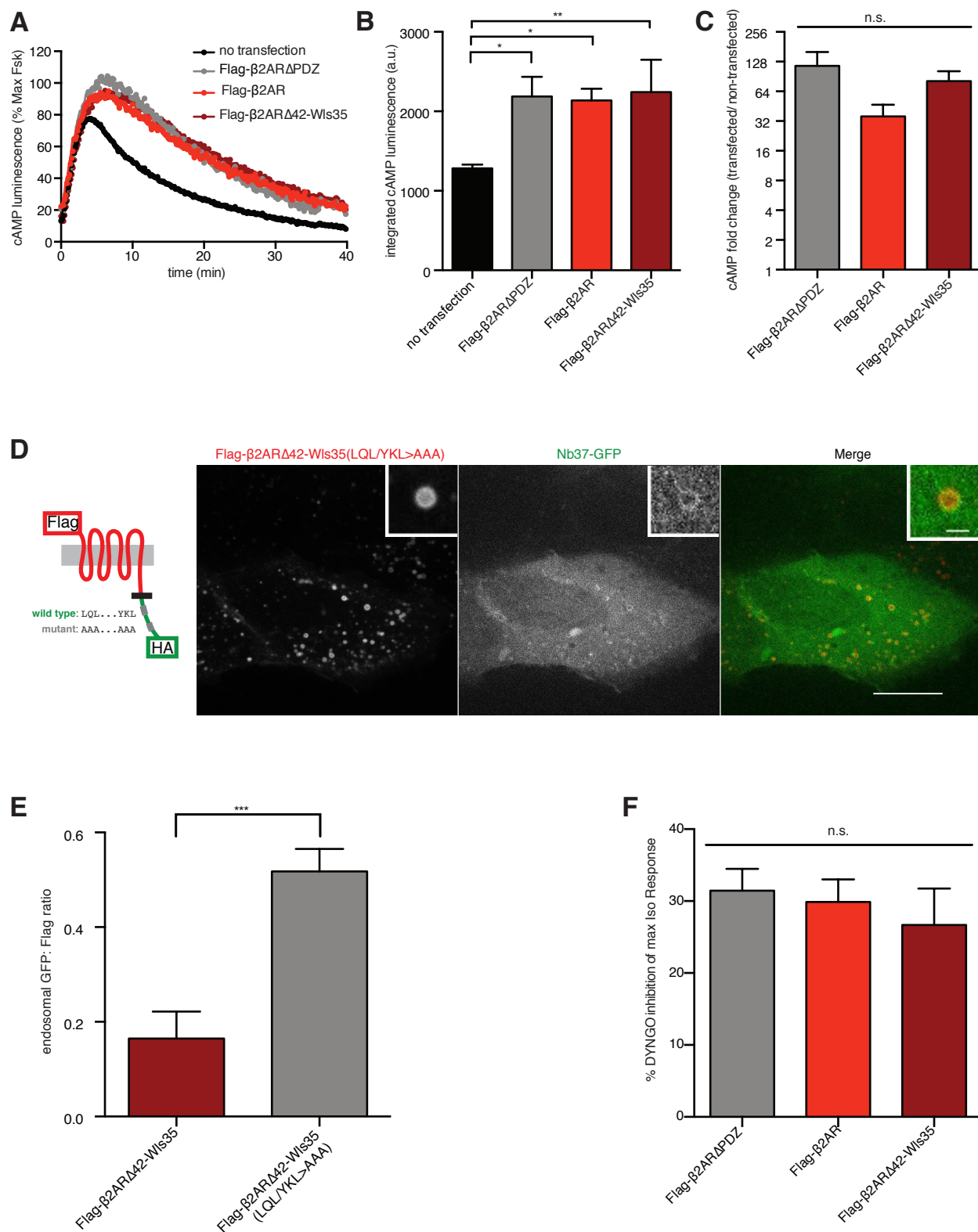


**Figure S6.** B2AR mutant constructs are functional in signaling assays and do not significantly alter the fraction cAMP produced from endosomes.

## **Chapter 3: Discussion**

### **3.1 Cargos with divergent itineraries exit endosomes together**

We set out to test whether retromer plays an instructive role in determining cargo destination after endosome exit. A model in which cargos are segregated by retromer prior to endosome exit has been widely proposed (Johannes & Wunder 2011; van Weering et al. 2010), based on the fact that different cargos require distinct accessory proteins and appear morphologically distinct on endosomal subdomains (Harterink et al. 2011). To the contrary, we found that B2AR and WIs, model recycling and retrograde transport cargos transit the same endosomes and exit endosomes together on vesicles formed by shared retromer endosome domains.

To our knowledge, this is the first time that the post-endocytic trafficking of recycling and retrograde transport cargos have been directly compared in the same cells. It is important to note that we did observe morphological differences in the appearance of each cargo on endosomal subdomains. WIs was previously described as appearing “vesicular” in morphology on retromer-marked endosomal domains (Harterink et al. 2011), while B2AR was described as “tubular” (Temkin et al. 2011). We also observed these distinct morphologies, but when the images are overlaid, it was clear that the large majority (>75%) of retromer endosome domains containing each cargo overlapped.



We believe that the distinct morphologies observed are due to the large differences cargo enrichment in retromer endosome domains (REDs). We found that the vast majority (>95%) of REDs containing both cargos were more highly enriched for WIs than B2AR. The relative enrichment of cargo in the RED versus endosome membrane was, on average, about 5 fold higher for WIs than B2AR.

Importantly, recycling and retrograde transport cargos were also observed exiting endosomes together. Endosome exit events were observed as REDs undergoing scission from the endosome, forming small vesicles that move independently from the remaining endosome. Generally, when these REDs contained both cargos, so did the exiting vesicles. Additionally, differences in cargo enrichment in REDs were maintained until after the RED scission event.

It is important to note we verified in our system that B2AR and WIs display their divergent and retromer-dependent trafficking itineraries. B2AR was found cycle between endosomes and the plasma membrane upon agonist addition and to accumulate at the plasma membrane (recycle) upon agonist removal. In contrast, WIs surface labeled at the plasma membrane transited endosomes and then accumulated at the TGN over long chase times, verifying its retrograde transport itinerary.

Together, these data show that B2AR and WIs, model cargos with divergent, retromer-dependent trafficking itineraries, traverse the same endosomes and the same

REDs, yet are distinct in their abilities to enrich in REDs. These data show that divergent cargos are not separated into distinct transport vesicles prior to endosome exit, but instead display a novel form of physical segregation in their abilities to enrich in and exit from REDs.

### **3.2 Cargo-retromer interaction motifs are interchangeable in achieving each cargo's downstream destination**

We next tested the second prediction of the model in which retromer plays an instructive role in determining cargo itinerary downstream of exit-- that retromer can biochemically distinguish cargos with distinct downstream destinations prior to endosome exit. To do so, we first investigated the modes of retromer connectivity of B2AR and Wls.

B2AR has a PDZ motif that links it to retromer through the accessory protein SNX27 (Cao et al. 1999; Lauffer et al. 2010; Temkin et al. 2011). When B2AR's PDZ motif is removed or disrupted, B2AR does not efficiently recycle or enter REDs (Cao et al. 1999; Lauffer et al. 2010; Temkin et al. 2011). Wls does not possess a consensus PDZ motif, nor does it exhibit impaired retromer-dependent trafficking when an epitope is added to its cytoplasmic tail, as observed with B2AR (Cao et al. 1999; Lauffer et al. 2010; Temkin et al. 2011). Wls is known to require a distinct accessory protein, SNX3 (Harterink et al. 2011; Zhang et al. 2011), but the motif within Wls that is required for its RED entry and retrograde transport was unknown prior to our work.

Therefore, we set out to determine the motif within Wls that is recognized by retromer. We found that Wls' cytoplasmic tail contains two consensus  $\Phi$ -X-[L/M] motifs (where  $\Phi$  is any hydrophobic amino acid) that necessary for strong RED enrichment and post-endocytic accumulation in the TGN.  $\Phi$ -X-[L/M] motifs have been extensively

characterized in a splice isoform of a distinct retromer cargo, the divalent metal transporter 1-II (DMT1-II) (Tabuchi et al. 2010), and a similar motif has also been described in the classical retromer cargo, the cation-independent mannose phosphate receptor (CI-MPR; (Seaman 2007). Within WIs, both of these motifs were conserved across all vertebrate species examined except zebrafish, in which the hydrophobic residue was replaced for threonine in the first motif. Interestingly, in the invertebrate species analyzed, each contained two motifs conforming the the alternate motif found in zebrafish, [S/T]-X-[L/M], indicating that this alternate motif may be an ancestral retromer binding motif. Tabuchi et al. showed that the  $\Phi$ -X-[L/M] motif is required for the DMT1-II cytoplasmic tail to interact with the purified retromer complex, suggesting that the interaction between this motif and retromer is direct.

These data suggest that B2AR and WIs interact with retromer through distinct mechanisms, utilizing distinct cargo-retromer interaction motifs. B2AR's PDZ motif interacts with the PDZ domain in SNX27 (Cao et al. 1999; Lauffer et al. 2010). SNX27 interacts directly with the VPS26 subunit of retromer and, interestingly, the interaction of SNX27 with VPS26 enhances SNX27's affinity for PDZ motifs (Gallon et al. 2014). In contrast, we found that WIs requires two  $\Phi$ -X-[L/M] motifs in its cytoplasmic tail for efficient RED entry and retrograde transport. It seems likely that this motif allows WIs to interact directly with retromer, rather than requiring an adaptor protein based work by Tabuchi et al. It is interesting to note that while DMT1-II has a single  $\Phi$ -X-[L/M] motif, WIs has two and that each are partially sufficient for its strong RED enrichment and

post-endocytic TGN delivery. An interesting avenue for future study would be to determine biochemical basis for the interaction between  $\Phi$ -X-[L/M] motifs and retromer and the stoichiometry of retromer subunits to the WIs tail.

Once cargo-retromer interaction motifs that were necessary RED entry and endosome exit for were identified in both B2AR and WIs, we next asked whether these motifs were also sufficient for divergent downstream targeting. We found, using chimeric mutant receptors, that the cargo-retromer interaction motifs from each cargo were sufficient for their characteristic degrees of RED enrichment; B2AR with WIs' cytoplasmic tail enriched strongly in REDs, while WIs with B2AR's cytoplasmic tail enriched weakly. However, the chimeric receptors also revealed that cargo-retromer interaction motifs do not determine the downstream itinerary of each cargo; B2AR with WIs' cytoplasmic tail recycled efficiently and WIs with B2AR's cytoplasmic tail underwent efficient retrograde transport.

This surprising result indicated that neither cargo-retromer interaction motifs nor degree of RED enrichment determined the downstream trafficking itinerary of cargos. This further refutes the model in which retromer plays an instructive role in specifying downstream destination of cargos. Instead, our results suggest that retromer cargos can interchangeably use cargo-retromer interactions motifs and transit the same endosomes and REDs to achieve divergent trafficking itineraries.

### **3.3 Distinct RED enrichments determine cargo delivery kinetics and signal activation at endosomes**

Because the degree of RED enrichment did not impact downstream cargo delivery destination, we wondered if they might have distinct effects.

First, we asked if distinct RED enrichments are indicative of different rates of endosome exit and, therefore, different rates downstream cargo delivery. Indeed, we found that cargos with weak RED enrichment, conferred by the B2AR tail, had slower delivery kinetics than cargos with strong RED enrichment, mediated by the WIs tail, to both the recycling and retrograde transport pathways.

Second, we asked about the effects of RED enrichment on GPCR signaling from endosomes. As B2AR had been shown to signal from endosomes (Irannejad et al. 2013), we were particularly intrigued how B2AR's relatively weak ability to enrich in REDs might affect its signaling. By comparing B2AR constructs with distinct RED enrichments, we found that the RED enrichment did not affect B2AR's ability to take on an active conformation at endosomes, but was inversely correlated with its ability to activate G $\alpha$ s at endosomes. This is consistent with previous reports that retromer terminates cAMP signaling of other GPCRs at the endosome membrane (Feinstein et al. 2013; Feinstein et al. 2011). Additionally, it is consistent with previous reports that enhanced endosomal dwell time causes enhanced G protein-mediated signaling from

endosomes (Chan et al. 2016; Tian et al. 2016a). Mechanistically, sequence-dependent enrichment of B2AR in REDs could attenuate Gs activation by physically preventing  $\beta$ 2AR coupling to Gs, perhaps through interaction with VPS26, which structurally resembles  $\beta$ -arrestin (Shi et al. 2006). Alternatively,  $\beta$ 2AR enrichment in REDs could attenuate endosomal Gs activation as a consequence of enhanced receptor endosome exit rate, and accordingly reduced residence time of activated  $\beta$ 2AR in endosomes. We presently favor the latter hypothesis because  $\beta$ 2AR has been explicitly shown to bind at endosomes to ARRDC3, an arrestin domain-containing protein that is distinct from VPS26 and which slows, rather than accelerates, receptor exit from endosomes. Importantly, ARRDC3 enhances the strength of  $\beta$ 2AR-elicited Gs activation in endosomes (Tian et al. 2016b). Thus it presently appears that the strength of endosomal G protein activation correlates with the residence time of  $\beta$ 2AR in endosomes, rather than with physical association with an arrestin-like protein. Accordingly, we propose that kinetic sorting executed by retromer at the level of cargo exit from endosomes, in addition to influencing downstream trafficking rates, reveals a discrete cellular mechanism by which endosomal signal activation is controlled.

Recently, it was reported that entrance into retromer-marked domains is required for B2AR's activation of G $\alpha$ s at endosomes (Bowman et al. 2016). While we also observe that the biosensor for G $\alpha$ s activation, nanobody37-GFP, preferentially localizes to REDs, it is unclear if this localization is indicative of the site of activation. Additionally, our results suggest the opposite, that B2AR in REDs is unable to activate G $\alpha$ s. Further

investigation to resolve the disagreements of these results is an interesting future direction. Nonetheless, the present results provide new insight to the link between retromer and GPCR signaling and reveal a previously unrecognized aspect of endosome signal regulation conferred by cargo-specific retromer sorting determinants.



### 3.4 Proposed mechanisms for sorting downstream of endosome exit

The ability of  $\beta$ 2AR and WIs to achieve cargo-appropriate trafficking itineraries after shared endosome exit via REDs implies that additional sorting must occur downstream of endosome exit. We think it is likely that multiple downstream sorting operations contribute and that the present observations provide a framework for these operations. Our proposed framework involves five main elements.

First, we show that both B2AR and WIs can rapidly transit to the plasma membrane after endocytosis and demonstrate that both cargos are present in the same fusing vesicles. These are hallmarks of retromer-dependent B2AR recycling as shown previously to occur directly from endosomes and while bypassing TGN or Golgi intermediates (Yudowski et al. 2006), thereby suggesting that both cargos can transit the direct recycling route at least to some degree. Further, we note that the relative brightness of SpH-WIs insertion actually exceeds that of SpH-B $\beta$ 2AR, when normalized to the ambient plasma membrane surround ( $\Delta F/F_0$  measurement). This is consistent with WIs's consistent tendency to accumulate in REDs and RED-derived exit vesicles in higher relative concentration than B2AR, and suggests that the source of these shared insertion events is the endosome-derived exit carriers themselves. It is interesting to note that the physiologically relevant itinerary of the DMT1-II iron transporter, a retromer cargo that utilizes a  $\Phi$ -X-[L/M] motif, is recycling to the plasma membrane (Tabuchi et al. 2010). While it has not been determined to what degree DMT1-II recycling occurs

indirectly via the TGN or directly to the plasma membrane, we speculate that direct recycling similar to that established for  $\beta$ 2AR may be a more widespread function of mammalian retromer. This particular consideration notwithstanding, it appears that DMT1-II provides a naturally occurring example of the ability of discrete retromer sorting determinants to support both retrograde and recycling itineraries.

Second we verify, as reported recently by others (Lee et al. 2016), that FAM21 depletion produces detectable TGN accumulation of the PDZ motif-directed  $\beta$ 2AR. Importantly, the mechanism by which FAM21 normally suppresses  $\beta$ 2AR localization to TGN is thought to involve a distinct effect of FAM21 on the phosphoinositide composition of the TGN, separate from its role as part of the WASH complex regulating local actin polymerization on endosomes (Lee et al. 2016; Derivery et al. 2009; Jia et al. 2010). Supporting this previous conclusion, and important to the present interpretation, FAM21 depletion produced no detectable change in the behavior of either model cargo at the endosome or RED.

Third, our chimeric mutant analysis clearly indicates that differences in the steady state itineraries of WIs relative to  $\beta$ 2AR are generated by structural determinants located outside of the specific sequences defined in the cytoplasmic tails of each cargo, and thereby likely involve sorting events that are independent of retromer or retromer-associated accessory proteins. Further supporting this view, we also show that HA-WIs $\Delta$ 35, despite lacking its retromer sorting determinant and thus being unable to

exit endosomes or undergo detectable delivery to TGN from the endocytic pathway, has a tendency to accumulate in TGN from the biosynthetic pathway. While the precise nature of this relative bias for WIs to accumulate in TGN remains unknown, it is interesting to note that  $\beta$ 2AR and WIs differ considerably in the length of their transmembrane domains: 23 amino acids for  $\beta$ 2AR and for 21 amino acids for WIs. These correspond closely to the average transmembrane domain lengths of plasma membrane and Golgi resident proteins in mammalian cells (Sharpe et al. 2010), and differences in transmembrane length of this order have been demonstrated previously to be sufficient to shift steady state cargo localization from plasma membrane to TGN or Golgi distributions (Masibay et al. 1993). Thus, it is conceivable that WIs has an inherent preference for accumulating in the TGN due to its distinct transmembrane core thickness when compared to  $\beta$ 2AR.

Fourth, wild type WIs has a dibasic motif located in its distal cytoplasmic tail that is distinct from the  $\Phi$ -X-[L/M] motifs shown here to be required for retromer-mediated exit from endosomes, and which mediates a discrete, retromer-independent process of Golgi-to-ER retrieval (Yu et al. 2014). We deliberately disabled this motif in the WIs-derived model cargos examined in the present study, to focus on the upstream step of retromer-dependent cargo exit from endosomes. However, we verified that this downstream retrieval step is indeed sufficient to almost completely sequester wild type WIs in the ER. Thus it is likely that this retromer-independent retrieval step plays a

major role in distinguishing the downstream itinerary of Wls from  $\beta$ 2AR under normal physiological conditions.

Fifth, the ability of Wls present in the plasma membrane to undergo rapid and constitutive endocytosis via clathrin-coated pits, directed by a Y-X-X- $\Phi$  motif present in the Wls third intracellular loop (Gasnereau et al. 2011), provides a means by which Wls that is delivered (or 'misdelaivered') to the plasma membrane could be retrieved and sorted again. Accordingly, constitutive endocytosis of Wls would enable an error-checking function of the sorting network and allow the physiologically appropriate retrograde itinerary of Wls to be repeatedly corrected and refined through iteration.

### 3.5 A distinct Wls cytoplasmic tail

Wls has an alternate splice variant in primates, Wls variant 2 (Wls2), which differs only in its distal cytoplasmic tail and 3' UTR (Figure 1A, Yu et al. 2014; Anon n.d.). Wls2 was shown by Yu et al. shown to be widely expressed in human tissues and in HeLa cells. Additionally, Yu et al. observed that the localization of Wls2 was distinct from Wls-- Wls2 localized to the plasma membrane and cytoplasmic vesicles rather than at the TGN (Yu et al. 2014). Yu et al. attributed the differences in localization between Wls and Wls2 to the fact that Wls2 lacks the C-terminal ER retrieval motif (Yu et al. 2014). It is important to note that in addition to lacking its ER retrieval motif, Wls2 also lacks the  $\Phi$ -X-[L/M] motifs required for efficient endosome exit and TGN accumulation.

I cloned a version of Wls that contains the distinct coding sequence of Wls2, but not the distinct 3' UTR, and includes an HA epitope in the first extracellular loop (HA-Wls2). I also observed that HA-Wls2 has a distinct localization pattern from HA-Wls; HA-Wls2 localizes largely to the plasma membrane and internal vesicles that largely co-localize with B2AR-positive endosomes, both at steady state and after surface chase (Figures 1B and 1C). Additionally, HA-Wls2 appears to enter the vast majority of B2AR-positive REDs (>85%; Figure 1D). However, the enrichment of HA-Wls2 in REDs appears weaker than HA-Wls, and looks very similar to that of Flag-B2R (Figures 1C and 1D). Consistent with this, we did not observe bright, frequent SpH-Wls2 plasma membrane insertions events, as was observed for SpH-Wls (data not shown). This localization

consistent with Wls2 lacking the  $\Phi$ -X-[L/M] motifs required for strong RED enrichment and efficient retrograde transport.

Another reason that Wls2 was particularly intriguing is that its distal cytoplasmic tail conforms to a PDZ motif. The distal three amino acids of Wls 2 are S-G-I, which conforms to the class I PDZ motif consensus sequence [S/T]-X- $\Phi$  (Beuming et al. 2005; Anon n.d.). Therefore, we hypothesized that Wls2 shows similar localization and trafficking to B2AR because it engages SNX27 through this PDZ motif. However, when the PDZ motif of Wls2 is removed (HA-Wls2 $\Delta$ PDZ), we did not observe a significant change in the localization of Wls2 at steady state (Figure 2A). Additionally, Braden Lobingier, a postdoctoral fellow in the lab, performed anisotropy assays to determine the dissociation constants for SNX27 binding to the Wls2 PDZ motif compared to the PDZ motifs of known interactors. These data showed that SNX27 binding to the Wls2tail has a higher much dissociation constant than the PDZ motifs of both PTH1R and B2AR, indicating a weaker affinity. Together, these data suggest that Wls2 is unlikely to interact with SNX27 in a manner that would alter its trafficking itinerary.

As it is unlikely that Wls2 engages retromer through either  $\Phi$ -X-[L/M] or PDZ motifs, we wondered if this protein is able to exit endosomes at all. Interestingly, live cell imaging of surface labeled HA-Wls2 revealed an interesting appearance of Wls at endosomes: Wls2 endosomes were frequently large and showed Wls2 internal vesicles that moved

with the endosomes, indicative of multivesicular bodies (Fig 2C, image series not shown).

The distinct sequence of the Wls2 cytoplasmic tail, which contains neither  $\Phi$ -X-[L/M] motifs nor ER retrieval motifs, is unlikely to function like Wls in Wnt transport from the ER/ Golgi to the extracellular space. Indeed, Yu et al. showed that Wls2 does not support efficient Wnt secretion (Yu et al. 2014). Wls2 undergoes endocytosis and is then unable to strongly accumulate in REDs, and it appears that the protein instead is present on intra-lumenal vesicles. Based on these data, I propose two potential alternative functions of Wls2.

First, it is possible that the Wls2-positive multivesicular bodies fuse to the plasma membrane, secreting the intra-lumenal vesicles as exosomes. Indeed, Wnt proteins have been reported on exosomes and these exosomes have also been reported to contain Wls (Gross et al. 2012; Korkut et al. 2009). Because Wnt ligands are extremely hydrophobic, the secretion of Wnt ligands on exosomes may allow the ligands to travel large distances. Interestingly, exosomes containing Wnt ligands and Wls have been reported in both *Drosophila* and human cells. *Drosophila* Wls also has an alternative splice isoform, Wls-long, which contains extra amino acids in its final intracellular loop which disrupt the protein's Y-X-X- $\Phi$  motif required for endocytosis (Koles & Budnik 2012). Unlike the primate Wls2 however, Wls-long can support Wnt secretion in *Drosophila*. The involvement of both the primate and *Drosophila* alternative Wls

isoforms in exosome secretion of Wnt ligands is an interesting direction for future studies.

A second possibility is that Wls2 functions in ligand-dependent antagonism of Wnt signaling. This concept was described in the hedgehog (Hh) signaling pathway, in which a distinct transmembrane protein, Hedgehog-interacting protein 1 (Hhip1), binds to Hh ligands and prevents their spreading (Jeong & McMahon 2005). As Hh signaling is dependent on gradients of Hh ligands, as does Wnt signaling (Wodarz & Nusse 1998), this regulation of signaling dramatically impacts cell fate decisions (Jeong et al. 2004). Wls2 could function like Hhip1, to bind to Wnt proteins on the cell surface and prevent their spreading. The endogenous Wls protein with its intact ER retrieval motif is very weakly localized to the plasma membrane, while it appears that Wls2 localization there is much more pronounced. It is also possible the Wls2 could have a more dramatic effect on the removal of Wnt ligands from the extracellular space by binding to them and then undergoing endocytosis and uptake into intra-lumenal vesicles, causing the degradation of the Wnt ligands. This possibility is another area that would make for an interesting future study.



### 3.6 References

Anon, RefSeq: NP\_001002292. Available at:

[http://www.genome.jp/dbget-bin/www\\_bget?refseq:NP\\_001002292](http://www.genome.jp/dbget-bin/www_bget?refseq:NP_001002292) [Accessed September 23, 2016a].

Beuming, T. et al., 2005. PDZBase: a protein-protein interaction database for PDZ-domains. *Bioinformatics* , 21(6), pp.827–828.

Bowman, S.L., Shiwarski, D.J. & Puthenveedu, M.A., 2016. Distinct G protein-coupled receptor recycling pathways allow spatial control of downstream G protein signaling. *The Journal of cell biology*. Available at: <http://dx.doi.org/10.1083/jcb.201512068>.

Cao, T.T. et al., 1999. A kinase-regulated PDZ-domain interaction controls endocytic sorting of the beta2-adrenergic receptor. *Nature*, 401(6750), pp.286–290.

Chan, A.S.M. et al., 2016. Sorting nexin 27 couples PTHR trafficking to retromer for signal regulation in osteoblasts during bone growth. *Molecular biology of the cell*, 27(8), pp.1367–1382.

Derivery, E. et al., 2009. The Arp2/3 activator WASH controls the fission of endosomes through a large multiprotein complex. *Developmental cell*, 17(5), pp.712–723.

Feinstein, T.N. et al., 2013. Noncanonical control of vasopressin receptor type 2

signaling by retromer and arrestin. *The Journal of biological chemistry*, 288(39), pp.27849–27860.

Feinstein, T.N. et al., 2011. Retromer terminates the generation of cAMP by internalized PTH receptors. *Nature chemical biology*, 7(5), pp.278–284.

Gallon, M. et al., 2014. A unique PDZ domain and arrestin-like fold interaction reveals mechanistic details of endocytic recycling by SNX27-retromer. *Proceedings of the National Academy of Sciences of the United States of America*, 111(35), pp.E3604–13.

Gasnereau, I. et al., 2011. Identification of an endocytosis motif in an intracellular loop of Wntless protein, essential for its recycling and the control of Wnt protein signaling. *The Journal of biological chemistry*, 286(50), pp.43324–43333.

Gross, J.C. et al., 2012. Active Wnt proteins are secreted on exosomes. *Nature cell biology*, 14(10), pp.1036–1045.

Harterink, M. et al., 2011. A SNX3-dependent retromer pathway mediates retrograde transport of the Wnt sorting receptor Wntless and is required for Wnt secretion. *Nature cell biology*, 13(8), pp.914–923.

Irannejad, R. et al., 2013. Conformational biosensors reveal GPCR signalling from endosomes. *Nature*, 495(7442), pp.534–538.

Jeong, J. et al., 2004. Hedgehog signaling in the neural crest cells regulates the

patterning and growth of facial primordia. *Genes & development*, 18(8), pp.937–951.

Jeong, J. & McMahon, A.P., 2005. Growth and pattern of the mammalian neural tube are governed by partially overlapping feedback activities of the hedgehog antagonists patched 1 and Hhip1. *Development*, 132(1), pp.143–154.

Jia, D. et al., 2010. WASH and WAVE actin regulators of the Wiskott-Aldrich syndrome protein (WASP) family are controlled by analogous structurally related complexes. *Proceedings of the National Academy of Sciences of the United States of America*, 107(23), pp.10442–10447.

Johannes, L. & Wunder, C., 2011. The SNXy flavours of endosomal sorting. *Nature cell biology*, 13(8), pp.884–886.

Koles, K. & Budnik, V., 2012. Exosomes go with the Wnt. *Cellular logistics*, 2(3), pp.169–173.

Korkut, C. et al., 2009. Trans-synaptic transmission of vesicular Wnt signals through Evi/Wntless. *Cell*, 139(2), pp.393–404.

Lauffer, B.E.L. et al., 2010. SNX27 mediates PDZ-directed sorting from endosomes to the plasma membrane. *The Journal of cell biology*, 190(4), pp.565–574.

Lee, S. et al., 2016. FAM21 directs SNX27–retromer cargoes to the plasma membrane by preventing transport to the Golgi apparatus. *Nature communications*, 7, p.10939.

Masibay, A.S. et al., 1993. Mutational analysis of the Golgi retention signal of bovine beta-1,4-galactosyltransferase. *The Journal of biological chemistry*, 268(13), pp.9908–9916.

Seaman, M.N.J., 2007. Identification of a novel conserved sorting motif required for retromer-mediated endosome-to-TGN retrieval. *Journal of cell science*, 120(Pt 14), pp.2378–2389.

Sharpe, H.J., Stevens, T.J. & Sean, M., 2010. A Comprehensive Comparison of Transmembrane Domains Reveals Organelle-Specific Properties. *Cell*, 142(1), pp.158–169.

Shi, H. et al., 2006. The retromer subunit Vps26 has an arrestin fold and binds Vps35 through its C-terminal domain. *Nature structural & molecular biology*, 13(6), pp.540–548.

Tabuchi, M. et al., 2010. Retromer-mediated direct sorting is required for proper endosomal recycling of the mammalian iron transporter DMT1. *Journal of cell science*, 123(5), pp.756–766.

Temkin, P. et al., 2011. SNX27 mediates retromer tubule entry and endosome-to-plasma membrane trafficking of signalling receptors. *Nature cell biology*, 13(6), pp.715–721.

Tian, X. et al., 2016a. The  $\alpha$ -Arrestin ARRDC3 Regulates the Endosomal Residence Time and Intracellular Signaling of the  $\beta$ 2-Adrenergic Receptor. *The Journal of*

*biological chemistry*, 291(28), pp.14510–14525.

Tian, X. et al., 2016b. The  $\alpha$ -Arrestin ARRDC3 Regulates the Endosomal Residence Time and Intracellular Signaling of the  $\beta$ 2-Adrenergic Receptor. *The Journal of biological chemistry*. Available at: <http://dx.doi.org/10.1074/jbc.M116.716589>.

van Weering, J.R.T., Verkade, P. & Cullen, P.J., 2010. SNX-BAR proteins in phosphoinositide-mediated, tubular-based endosomal sorting. *Seminars in cell & developmental biology*, 21(4), pp.371–380.

Wodarz, A. & Nusse, R., 1998. Mechanisms of Wnt signaling in development. *Annual review of cell and developmental biology*, 14, pp.59–88.

Yudowski, G.A., Puthenveedu, M.A. & von Zastrow, M., 2006. Distinct modes of regulated receptor insertion to the somatodendritic plasma membrane. *Nature neuroscience*, 9(5), pp.622–627.

Yu, J. et al., 2014. WLS retrograde transport to the endoplasmic reticulum during Wnt secretion. *Developmental cell*, 29(3), pp.277–291.

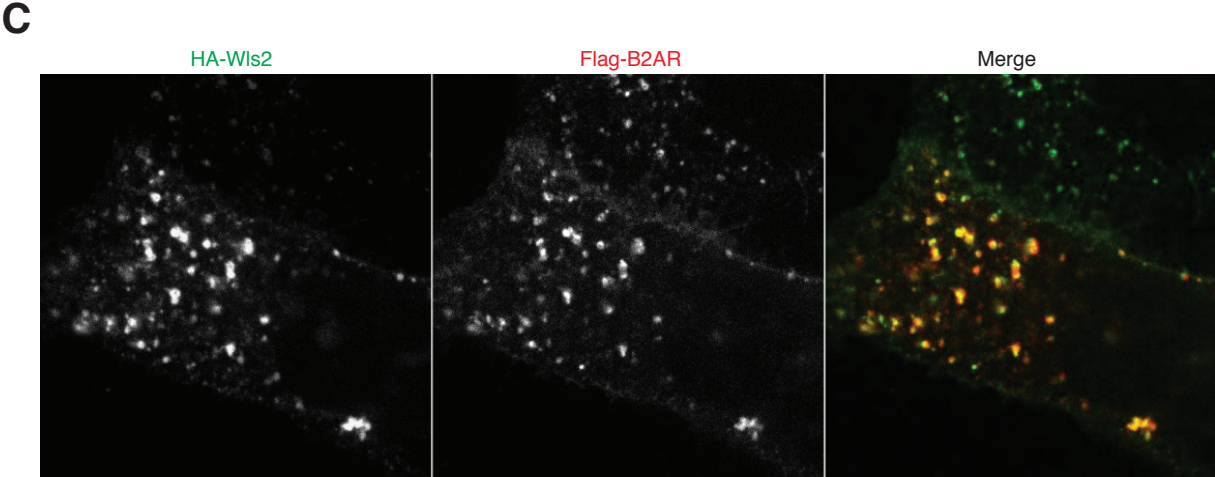
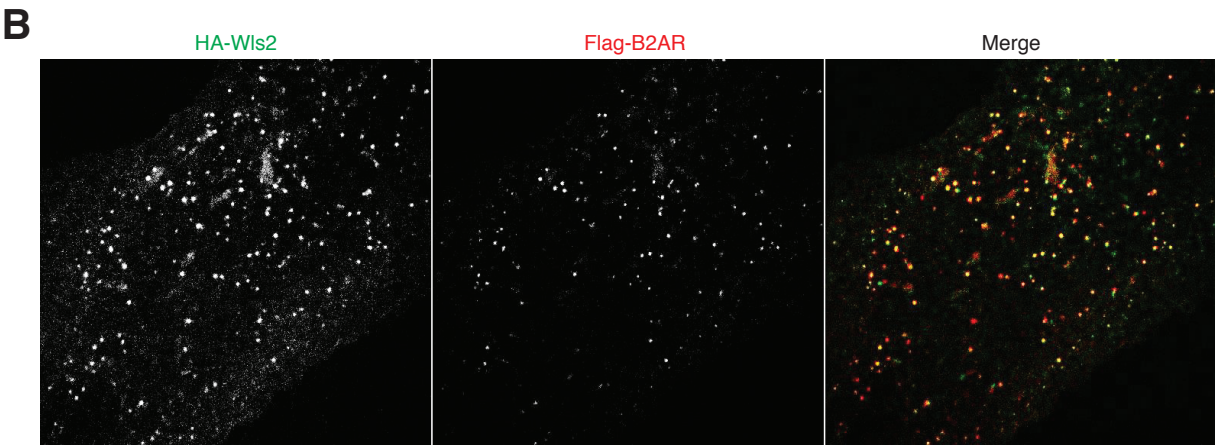
Zhang, P. et al., 2011. SNX3 controls Wingless/Wnt secretion through regulating retromer-dependent recycling of Wntless. *Cell research*, 21(12), pp.1677–1690.

### 3.7 Figures

**Figure 1. Wls2 trafficks differently than Wls.** (A) Amino acid sequences of the human Wls (upper) and Wls2 (lower) cytoplasmic tails. The sequences that diverge between isoforms are in bold and the consensus PDZ motif is italicized. (B) Representative confocal image of a fixed HeLa cell expressing HA-Wls2 and Flag-B2AR surface labeled with anti- HA and Flag antibodies following a 60 minute chase incubation. (C) Representative confocal image of a live HEK-293 cell expressing HA-Wls2 and Flag-B2AR surface labeled with anti- Flag and HA antibodies after subsequent chase incubation. (D) Enlarged views of endosomes in HEK-293 cells from cells prepared as in C with REDs containing both Wls2 and B2AR, only Wls2, or only B2AR. Quantification of percent of REDs containing each cargo is denoted to the right of each category as mean  $\pm$  standard deviation.  $n=2$  independent experiments.

**Figure 2. Examination of Wls2's PDZ motif and its localization on multivesicular bodies.** (A) Representative confocal images of fixed HeLa cells expressing HA-Wls2 or HA-Wls2 $\Delta$ PDZ and immunostained with anti- HA and Giantin antibodies. (B) Fluorescence anisotropy measurement of purified SNX27 and fluorescein labeled peptides. Experiment was performed by Braden Lobingier.  $n=1$ . (C) Representative image of a live HEK-293 cell expressing HA-Wls2 and Flag-B2AR surface labeled with anti- Flag and HA antibodies after subsequent chase incubation.

**A** Wls cytoplasmic tail:  
 APSHKKNYGEDQSNGLGVHSGEELQLTTTITHVDGPTEIYKLRKEAQE  
 Wls2 cytoplasmic tail:  
 APSHKKNYGEDQSNGMQLPCKSREDCALFVSELYQELFSASKYSFINDNAASGI



**D**

	Flag-B2AR	HA-Wls2	Merge	percent REDs containing (mean ± SD)
both cargos				88.2 ± 5.3
Wls2 only				4.9 ± 0.7
B2AR only				6.9 ± 4.2

**Figure 1.** Wls2 trafficks differently than Wls.

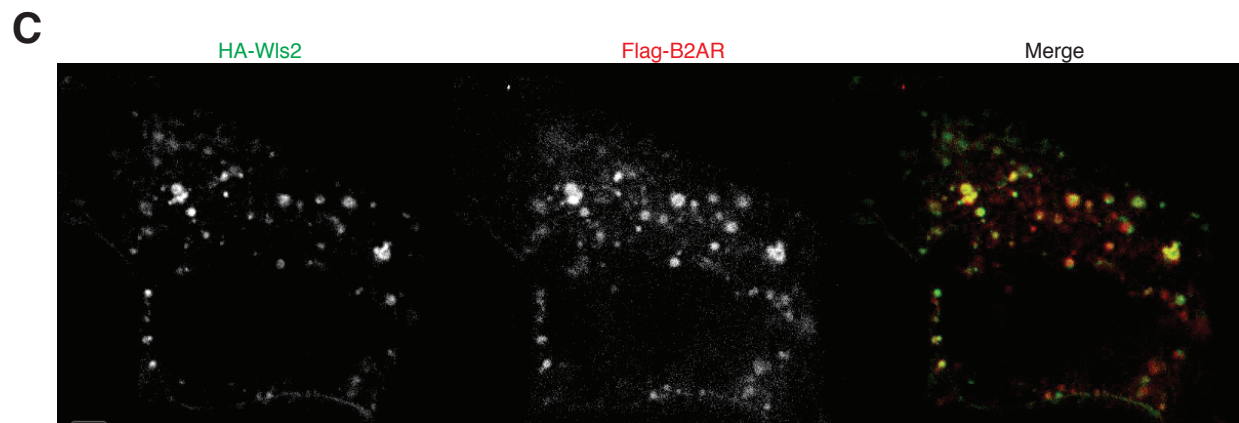
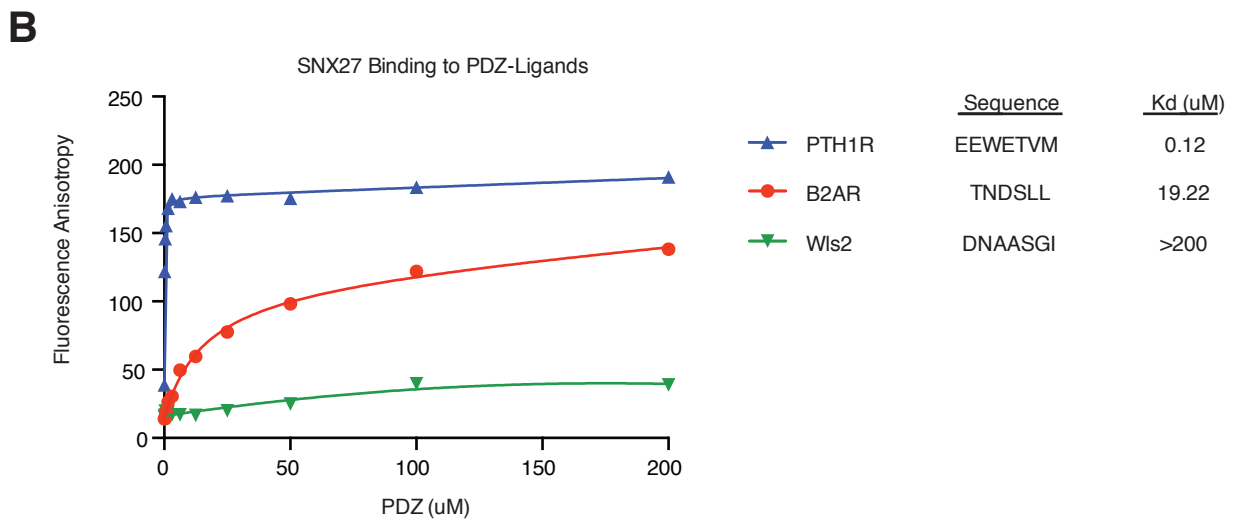
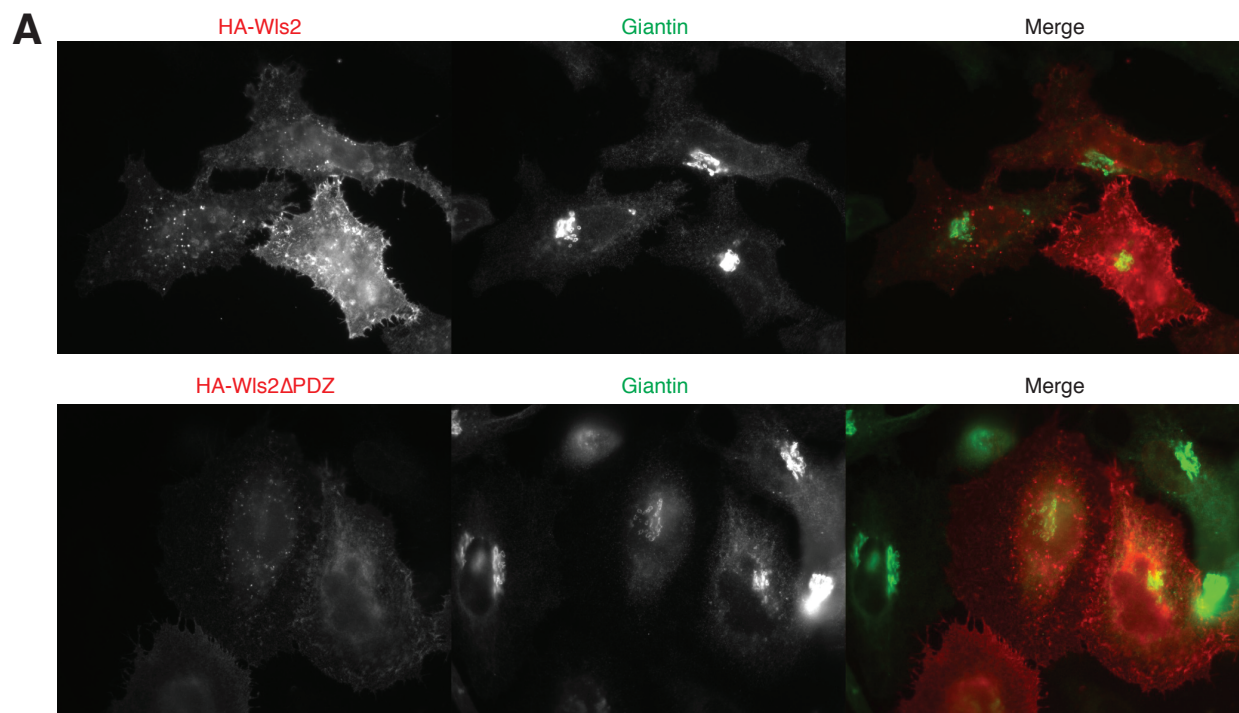


**Figure 2.** Examination of Wls2's PDZ motif and its localization on multivesicular bodies.

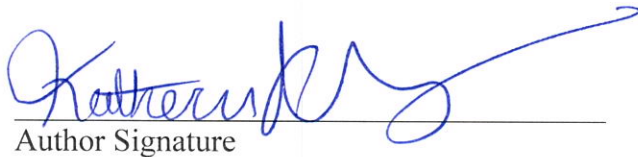


**Publishing Agreement**

*It is the policy of the University to encourage the distribution of all theses, dissertations, and manuscripts. Copies of all UCSF theses, dissertations, and manuscripts will be routed to the library via the Graduate Division. The library will make all theses, dissertations, and manuscripts accessible to the public and will preserve these to the best of their abilities, in perpetuity.*

***Please sign the following statement:***

*I hereby grant permission to the Graduate Division of the University of California, San Francisco to release copies of my thesis, dissertation, or manuscript to the Campus Library to provide access and preservation, in whole or in part, in perpetuity.*

  
\_\_\_\_\_  
Author Signature

9/29/16  
Date